The Dissertation Committee for Aditya Aravind
certifies that this is the approved version of the following dissertation:

Modeling and Constraining Inflationary and Pre-Inflationary Eras

Committee:

Sonia Paban, Supervisor

Willy Fischler

Jacques Distler

Can Kilic

Paul R. Shapiro

Modeling and Constraining Inflationary and Pre-Inflationary Eras

by

Aditya Aravind, B.Tech.

DISSERTATION

Presented to the Faculty of the Graduate School of

The University of Texas at Austin

in Partial Fulfillment

of the Requirements

for the Degree of

DOCTOR OF PHILOSOPHY

THE UNIVERSITY OF TEXAS AT AUSTIN

August 2016

Dedicated to my parents

Acknowledgments

There are many people who contributed in different ways to the research presented in this dissertation. I would like to acknowledge my gratitude to all these people for their direct and indirect contributions. Having said that, I shall list below a few of them whose contributions come foremost to my mind.

I would like to begin by thanking my supervisor Sonia Paban, for her unfailing support and guidance all through my graduate career. Apart from giving a general direction to my research, she also helped me find my way through many projects through her insight, experience and willingness to spend several hours in helpful discussions.

The time I spent at UT has been a great learning experience in many ways. I would like to thank all the professors of the theory group for creating an intellectually stimulating environment that enabled me to think more carefully and methodically about physics than I had ever done before. In particular, I would like to thank Vadim Kaplunovsky for his thorough introduction to quantum field theory and the world beyond, Can Kilic for patiently answering my often naive questions on collider physics and particle phenomenology, Willy Fischler for demonstrating how to tackle problems by thinking like a physicist and Jacques Distler for the many insightful comments and probing questions that redirected my approach to a research problem more than once.

The journey of research becomes all the more meaningful and enjoyable in the presence of colleagues and fellow researchers on the same road. I would like to thank all the former and current postdocs and students in the group (and some outside), the interactions with whom played a crucial role in my education. In particular, I would like to thank those whom I had most discussions with, Jiang-Hao Yu, Siva Swaminathan, Minglei Xiao, Sandipan Kundu, Dan Carney, Joel Meyers, Ely Kovetz, Brandon Dinunno, Anindya Dey, Jacob Claussen and others. Most of all, I would like to thank my long-time collaborator, Dustin Lorshbough, with whose help I acquired a major part of my knowledge in cosmology and whose approach to life and dedication to research has influenced me in so many different ways.

I would also like to express my sincere gratitude to Jan Duffy for her amazing efficiency in handling all administrative matters which converted (and continues to convert) many potential administrative nightmares into smooth affairs. I would also like to thank Abel Ephraim and Josh Perlman for their timely help with technical and computing issues.

Last, but not the least, I would like to thank my family, especially my parents, whose constant support and motivation prompted me to take up research and to keep working through the challenges; without their efforts none of this would have been possible.

The material presented in this dissertation is based upon work generously supported by the National Science Foundation under Grant Number PHY-1316033.

Modeling and Constraining Inflationary and Pre-Inflationary Eras

Aditya Aravind, Ph.D.
The University of Texas at Austin, 2016

Supervisor: Sonia Paban

The paradigm of cosmic inflation has had great success in explaining the statistical properties of fluctuations in the Cosmic Microwave Background (CMB). In this dissertation we discuss a few avenues for modeling and constraining the inflationary universe - constraints on excited states of inflationary fluctuations, some aspects of multi-field tunneling and also constraints on and predictions from a specific model of inflation connecting Higgs physics and dark matter.

First, we show that in standard single field slow roll inflation, Bogoliubov excitations of the fluctuation spectrum are tightly constrained by observations. These constraints ensure that the squeezed limit non-gaussianity obtained from such excited states cannot be large. They also rule out any significant imprints in the CMB coming from a sudden transition from kinetic energy domination to inflation.

We then explore tunneling in the context of field theory, a scenario that has potential relevance to the pre-inflationary universe. We discuss subtleties involved in choosing the trajectory for tunneling out of a metastable vacuum in a multi-field potential. In particular, we use exact solutions and scaling relations to show that tunneling may happen along directions with large barriers, thus making the common intuition coming from quantum mechanical tunneling unreliable in estimating the tunneling trajectory and therefore, the bounce action.

We then explore a specific model of inflation that involves the addition of a scalar singlet and fermionic dark matter to the standard Higgs inflation scenario. We show that dark matter constraints and the requirement to support successful inflation significantly constrain the available parameter space for this model. We also find that the model generically predicts a small value of the tensor-to-scalar ratio r, similar to standard Higgs inflation, though it allows for a larger range of values for the scalar spectral tilt n_S.

Table of Contents

List of Tables

List of Figures

Chapter 1

Introduction

Observations of the Cosmic Microwave Background (CMB) indicate that the universe was nearly homogeneous and isotropic (up to fluctuations of $\mathcal{O}\left(10^{-5}\right)$) at the time of recombination. Since a universe undergoing decelerating expansion brings larger and larger comoving volumes (volumes expanding with the universe) within causal contact as time elapses, this would mean a much larger and possibly causally disconnected volume of the universe was homogeneous at times long before the recombination time. The considerable fine tuning required by this scenario is one of the strong motivations that suggested a period of accelerated expansion in the early universe, or "inflation", that could take a small region, causally connected to begin with, and cause it to expand enormously in a short period of time.

Apart from addressing the horizon and flatness problems as well as explaining the absence of the exotic contents in the present day universe, the paradigm of inflation has also proved to be greatly successful in explaining features in the spectrum of fluctuations in the CMB in a natural way. In fact, from a model-builder's point of view, it is a matter of some regret that many of the simplest models of inflation predict a spectrum of quantum fluctuations

that agree well with the latest constraints [2] based on CMB temperature fluctuation observations. Nevertheless, given the many ongoing and future experiments collecting CMB polarization and LSS data, and the many experiments that probe the early universe in other ways such as dark matter probes, there is much promise for tighter observational constraints on inflation models. In this dissertation we shall discuss some of the aspects of inflationary models and observational constraints on them.

The simplest models of inflation are the so-called "single-field slow roll" (SFSR) inflation models, where the universe is dominated by the energy density of a single scalar field called the "inflaton" (ϕ), and the period of accelerated expansion is driven by the potential energy of this scalar field which far exceeds its "slowly rolling" kinetic energy. The action can be written as

$$S = \int d^4x\sqrt{-g}\left[\frac{M_{\rm pl}^2}{2}R - \frac{1}{2}(\partial\phi)^2 - V(\phi)\right] . \tag{1.1}$$

Taking a homogeneous solution, we can write the background metric in the form

$$ds^2 = -dt^2 + a(t)^2 dx_i dx_i = a(t)^2(-d\tau^2 + dx_i dx_i) , \tag{1.2}$$

where τ is the conformal time and $a(t)$ the time-dependent scale factor of the universe.

The background equations of motion are as follows

$$3M_{\rm pl}^2 H^2 \;=\; \frac{1}{2}\dot{\phi}^2 + V(\phi) ,$$

$$
\begin{aligned}
M_{\rm pl}^2 \dot{H} &= -\frac{1}{2}\dot{\phi}^2 \,, \\
0 &= \ddot{\phi} + 3H\dot{\phi} + V'(\phi) \,,
\end{aligned}
\tag{1.3}
$$

where $H = H(t) = \dot{a}/a$ is the Hubble parameter and a dot over a quantity signifies derivative with respect to (real) time.

We then define the slow-roll parameter as

$$
\epsilon = -\frac{\dot{H}}{H^2} = \frac{1}{2}\frac{\dot{\phi}^2}{M_{\rm pl}^2 H^2} \,,
\tag{1.4}
$$

where the second equality holds only when the second equation in (1.3) is satisfied.

We can expand the above action about its classical solution to obtain the action up to second order in perturbations [91]. The metric perturbations can be characterized as [21]

$$
ds^2 = -(1+2\Phi)dt^2 + 2a(t)B_i\, dx^i\, dt + a(t)^2\left[(1-2\Psi)\delta_{ij} + 2E_{ij}\right] dx^i dx^j . \tag{1.5}
$$

The perturbations characterized above include scalar, vector and tensor components, and these components are generally gauge-dependent. Since physical observables should not depend on the choice of gauge, it is usually advisable to work with gauge invariant combinations of these perturbations. In the rest of this dissertation, we shall work with one specific gauge invariant scalar perturbation obtained by combining metric (curvature) and matter (field) perturbations, called comoving curvature perturbation ($\mathcal{R}$)

$$
\mathcal{R} = \Psi - \frac{H}{\dot{\phi}}\delta\phi \,.
\tag{1.6}
$$

The tensor component of E_{ij}, which we term as γ_{ij} is also gauge invariant.

The inflationary action expanded to second order in scalar perturbations can expressed in terms of the comoving curvature perturbation [91] as

$$S = M_{\rm pl}^2 \int dt\, d^3x\, \epsilon\, a^3 \left[\dot{\mathcal{R}}^2 - \frac{1}{a^2} (\partial \mathcal{R})^2 \right] . \tag{1.7}$$

On quantizing the system, we can write the action as

$$S_{\mathcal{R}} = -M_{\rm pl}^2 \int d^4x\, \epsilon\, a^3 \bar{g}^{\mu\nu} \partial_\mu \hat{\mathcal{R}} \partial_\nu \hat{\mathcal{R}} \,, \tag{1.8}$$

where

$$\hat{\mathcal{R}} = \int \frac{d^3k}{(2\pi)^3} \hat{\mathcal{R}}_k e^{i\vec{k}\cdot\vec{x}} \,. \tag{1.9}$$

The fourier space operator can be written in terms of creation and annihilation operators as

$$\hat{\mathcal{R}}_{\vec{k}} = \mathcal{R}_k \hat{a}^\dagger_{\vec{k}} + \mathcal{R}^*_k \hat{a}_{-\vec{k}} \,,$$

$$[\hat{a}_k, \hat{a}^\dagger_{k'}] = (2\pi)^3 \delta^3 \left(\vec{k} - \vec{k}' \right) . \tag{1.10}$$

Here, $\mathcal{R}_k = \mathcal{R}_k(t)$, also called the "mode function", is any solution to the equation of motion derived from the action (1.8)

$$\ddot{\mathcal{R}} + \left(3H + \frac{\dot{\epsilon}}{\epsilon} \right) \dot{\mathcal{R}} + \frac{k^2}{a^2} \mathcal{R} = 0 \,. \tag{1.11}$$

In this above equation, the Hubble parameter H, scale factor a, the slow-roll parameter ϵ and $\mathcal{R}$ are in general time dependent quantities. Normally, during inflation, ϵ is approximately time independent and therefore the $\dot{\epsilon}$ term can be ignored. However, in case of equation of state transitions, this term may become relevant.

The choice of mode function fixes the definition of creation and annihilation operators and therefore also fixes the "vacuum" state which is annihilated by the annihilation operator. The mode function that corresponds to the standard adiabatic vacuum is commonly known as the Bunch-Davies mode function $\mathcal{R}_{BD}$. This mode function can be written as

$$\mathcal{R}_k(t) = \mathcal{R}_{BD}(k,t) = \frac{1}{\sqrt{2k^3}} \frac{H}{\sqrt{2\epsilon} M_{\rm pl}} \left(1 + i\frac{k}{aH}\right) e^{-i\frac{k}{aH}} . \qquad (1.12)$$

For this choice of mode function, the power spectrum of fluctuations at late times ($k \ll aH$) can be calculated as the two-point function of the $\hat{\mathcal{R}}$ operator over the vacuum state

$$\begin{aligned} \langle \hat{\mathcal{R}}_k \, \hat{\mathcal{R}}_{k'} \rangle &= (2\,\pi)^3 \, \delta^3 \left(\vec{k} + \vec{k'}\right) P_{\mathcal{R}} \,, \\ P_{\mathcal{R}} &= |\mathcal{R}_{\mathcal{BD}}(k,t)|^2 = \frac{1}{2k^3} \frac{H^2}{2\epsilon M_{\rm pl}^2} \,, \\ \Delta^2_{\mathcal{R}} &= \frac{k^3}{2\pi^2} P_{\mathcal{R}} = \frac{1}{8\pi^2\epsilon} \frac{H^2}{M_{\rm pl}^2} \,. \end{aligned} \qquad (1.13)$$

A very similar discussion follows for the case of tensor modes γ_{ij}, where

we define the operator for the tensor fluctuations as

$$\hat{\gamma}_{ij} = \int \frac{d^3k}{(2\pi)^3} \sum_{s=\pm} \epsilon^s_{k,ij}\, \hat{\gamma}^s_{\vec{k}}\, e^{i\vec{k}\cdot\vec{x}}, \tag{1.14}$$

with the second order action and adiabatic solution (in fourier space) having slightly different forms

$$\begin{aligned} S_\gamma &= -\frac{M_{\rm pl}^2}{8} \int d^4x\ a^3 \bar{g}^{\mu\nu} \partial_\mu \hat{\gamma}_{ij} \partial_\nu \hat{\gamma}_{ij}\,, \\ \gamma^{(s)}_{k,BD}(k,t) &= \frac{1}{\sqrt{2k^3}} \frac{\sqrt{2}H}{M_{\rm pl}} \left(1 + i\frac{k}{aH}\right) e^{-i\frac{k}{aH}}\,. \end{aligned} \tag{1.15}$$

Therefore, the tensor power spectrum and tensor to scalar ratio for Bunch Davies scalar and tensor perturbations is obtained as

$$\begin{aligned} \Delta^2_\gamma &= \frac{2}{\pi^2} \frac{H^2}{M_{\rm pl}^2}\,, \\ r &= \frac{\Delta^2_\gamma}{\Delta^2_{\mathcal{R}}} = 16\epsilon\,. \end{aligned} \tag{1.16}$$

With this introduction to the standard notations and terminology used in the context of single field slow roll inflation, we are now ready to discuss the results presented in the following chapters.

In Chapter 2 we discuss excited initial states and the various bounds that constrain the excitations. Further, we discuss the implications of these bounds on CMB non-gaussianity and pre-inflationary kinetic energy dominated states. The content of this chapter is based primarily on results presented in [12, 13] which were later extended in [15].

In Chapter 3, we discuss our work on multi field tunneling [11, 14]. Tunneling transitions are among the many potential scenarios that could have preceded inflation, and they could possibly even have observable consequences if inflation did not last much longer than the minimal number of e-folds required to solve the horizon problem. However, our discussion is restricted to the background tunneling probability out of a metastable vacuum in a multi-field space in the absence of gravity; we do not go into the details of the perturbation spectrum generated by a tunneling event or the effects of gravity, which is ultimately necessary if we were to constrain such scenarios through cosmological observables. Research presented in this chapter was published in [11].

In Chapter 4, we discuss a specific model involving inflation driven by either a non-minimally coupled Higgs or a non-minimally coupled singlet scalar field with quartic coupling to the Higgs. Our model also includes fermionic dark matter coupled to the scalar singlet, and we study the viability of such a model in light of constraints from dark matter and collider physics apart from the constraints coming from requiring successful inflation. Research presented in this chapter was published in [16].

Finally, in Chapter 5, we conclude by summarizing the results presented in the preceding chapters and discussing our outlook for the future.

Chapter 2

Bogoliubov Excited Initial States[1]

2.1 Introduction

In the previous chapter, we showed the expression for the inflationary power spectrum obtained when the perturbations are in the Bunch-Davies state. While this choice may be well motivated, there is no reason why the perturbations must be constrained to be in the adiabatic vacuum [3–5, 32, 35, 36, 57, 63, 65, 73, 81, 82]. In this chapter, we discuss the scenario where the perturbations occupy Bogoliubov excited states and study the constraints on these states coming from observations. While these states are a subset of the possible states that could be occupied by the fluctuations [81, 82], they are motivated by the fact that that various pre-inflationary scenarios such as equation of state transitions can naturally take fluctuations into such excited states [15, 32].

The rest of this chapter is organized as follows. In Section 2.2, we introduce the parametrization of Bogoliubov excited states. Our method of bounding excited states is explained in Section 2.3. Afterwards, we discuss the implications of our bounds on non-gaussianity in Section 2.4 and on a

[1]Portions of this chapter have been previously published in [12, 13]

pre-inflationary physics model in Section 2.5. We summarize our discussion of excited states in Section 2.6.

2.2 Parametrization

A simple way of parametrizing Bogoliubov excited states is by moving to a new basis for the Fock space, or in other words performing a Bogoliubov transformation. By choosing a new mode function (and its conjugate) which is a linear combination of the existing mode function with its complex conjugate, we can choose new creation and annihilation operators which are also related to the existing ones by a linear combination [46]. The "vacuum" state in this basis, which is the state annihilated by the new annihilation operator, will be different from the Bunch-Davies vacuum and the new mode function will also be a solution to the equation of motion (1.11). In terms of Bogoliubov parameters α and β and the Bunch-Davies mode function (1.12), this new mode function can be written as as

$$\mathcal{R}_k(t) \;=\; \alpha(k)\mathcal{R}_{BD}(k,t) + \beta(k)\mathcal{R}^*_{BD}(k,t)\,, \tag{2.1}$$

with the normalization condition $|\alpha|^2 - |\beta|^2 = 1$. The magnitude of $\beta(k)$, therefore, parametrizes the departure of this state from the Bunch Davies state.

In this chapter we shall discuss bounds on Bogoliubov excited states coming from the observed CMB spectrum and their implications.

2.3 Bounds on Excited States

Standard SFSR inflation with Bunch-Davies fluctuations generically predicts a nearly scale-invariant power spectrum of fluctuations, and this is found to match well with observational data [2]. Therefore, any predictions coming from a model having excited fluctuations must not deviate too significantly from the approximate scale invariance of the power spectrum. The power spectrum amplitude for Bogoliubov excited states at late times can be written as

$$\Delta^2_{\mathcal{R}} = \frac{k^3}{2\pi^2} P_{\mathcal{R}} = \frac{k^3}{2\pi^2} \left|\mathcal{R}_k(t)\right|^2 \approx \frac{1}{8\pi^2\epsilon} \frac{H^2}{M^2_{\rm pl}} \left|\alpha + \beta\right|^2 . \tag{2.2}$$

Therefore, it is reasonable to require that $|\alpha + \beta|$ does not have a significant $k-$dependence. In principle, it may be possible for $|\alpha + \beta|$ to have a significant scale dependence that is exactly compensated by an appropriate time dependence of the background parameters in the theory (such as H and ϵ), since the horizon exit of different scales happen at different times. In the interest of simplicity and predictability, we ignore such fine tuning in this study and assume that $|\alpha + \beta|$ is (almost exactly) independent of k for all the modes visible in the CMB so that the predicted power spectrum lies within observed error bars.

Let us therefore consider the situation where the CMB is comprised entirely of excited modes with nonzero $\beta(k)$. In order for these modes to comprise the CMB and for inflation to successfully solve the horizon problem,

we require all the modes including the lowest-ℓ observed modes to be within the horizon at the beginning of inflation. Therefore, we get

$$p = \frac{k}{a} > H\,, \tag{2.3}$$

where p is the physical momentum of any mode that is visible in CMB and p, a and H are evaluated at the beginning of inflation. Since all the CMB modes must satisfy this bound, it is appropriate to write this constraint in terms of the momentum $p = p_{IR}$, corresponding to the lowest-ℓ mode in the CMB.

The next constraint we must impose is the backreaction constraint. Since we deal with excited modes, we must ensure that their energy density does not become large enough to significantly affect the background evolution of the universe. During inflation, the background potential energy of the inflaton dominates the energy density of the universe. Therefore, as long as the energy density contained in the fluctuations is much smaller than the background potential energy, we expect some form of inflation to happen [12]. However, if the fluctuation energy exceeds the background kinetic energy, then the second among the background equations of motion (1.3) can be significantly corrected, affecting the calculation of the second order action and the subsequent results. Therefore, in order to consistently satisfy all the background equations of motion, we must impose the condition that the energy density in the excitations is smaller than the background kinetic energy of the inflaton

[53]

$$\begin{aligned}\langle\rho_{\mathcal{R}}\rangle &= M_{\rm pl}^2\epsilon\int_0^{k_{\rm UV}}\frac{d^3k}{(2\pi)^3}\left[|\dot{\mathcal{R}}_k|^2-|\dot{\mathcal{R}}_{k,BD}|^2+\left(\frac{k}{a}\right)^2\left(|\mathcal{R}_k|^2-|\mathcal{R}_{k,BD}|^2\right)\right]\\ &= \frac{|\beta|^2}{8\pi^2}\left[p_{\rm UV}^4+\mathcal{O}\left(H^2p_{\rm UV}^2\right)\right]\\ &\ll \epsilon M_{\rm pl}^2H^2.\end{aligned} \tag{2.4}$$

Note that we have taken $\beta(k)$ to be approximately independent of k; the form of the integral indicates that the value of β for large k will have greater impact on the energy density. From this expression, we get the constraint

$$p_{UV} \ll \left(\frac{8\pi^2\epsilon M_{\rm pl}^2H^2}{|\beta|^2}\right)^{1/4}. \tag{2.5}$$

In order for excited states to comprise the CMB, the most conservative case with the least restrictive backreaction bound is when modes of momentum higher than the observed (CMB) modes are all in the Bunch-Davies state (not excited). In this case, p_{UV} corresponds to the physical momentum of the highest-ℓ CMB mode evaluated at the time at which the backreaction bound is imposed. This also means that p_{UV} is at about 3-4 orders of magnitude larger than p_{IR}.

Since the physical momentum scales as $1/a$, the energy density in the fluctuations drops off rapidly as $1/a^4$ during inflation. This also means that the backreaction constraint is the stricter at earlier times.

An important physical motivation for considering excited states is that they may be generated by some pre-inflationary phase/equation of state tran-

sition or other such phenomena. In such cases, there is a certain time at which inflation can be said to "begin", and the backreaction bound must be imposed at that time so that inflation begins (and continues) without problems. Therefore, it is appropriate for us to impose both the subhorizon and backreaction constraints simultaneously at the beginning of inflation (or at whatever time these fluctuations were excited). On doing so, we get

$$\begin{aligned} 10^3 H &\ll \left(\frac{8\pi^2 \epsilon M_{\rm pl}^2 H^2}{|\beta|^2}\right)^{1/4} \\ \implies 10^3 &\ll \left(\frac{1}{\Delta_{\mathcal{R}}^2}\frac{|\alpha+\beta|^2}{|\beta|^2}\right)^{1/4} \\ \implies |\beta| &< \frac{1}{10^6\left(\Delta_{\mathcal{R}}^2\right)^{1/2}}|\alpha+\beta|\,, \end{aligned} \tag{2.6}$$

where we have assumed $p_{UV} \geq 10^3\, p_{IR}$.

By substituting the measured value of $\Delta_{\mathcal{R}}^2$, we can see that this restricts excitation parameter β to be at most a percent level, $|\beta| < 0.022$, with $0.98 < |\alpha+\beta| < 1.02$.

2.4 Implications for Non-Gaussianity

As discussed in Appendix A, non-gaussianity is parametrized by the parameter f_{NL} which gives the relative magnitude of bispectrum (three-point function in momentum space) in relation to the square of the power spectrum. f_{NL} is calculated by fixing the template, i.e, the shape of the triangle formed by

the three momenta in the bispectrum, as local, equilateral or orthogonal. Observationally, the tightest constraints come from the squeezed/local template, f_{NL}^{local}, and as reported by Planck [2] has $\mathcal{O}(1)$ error bars,

$$f_{NL}^{local} = 0.8 \pm 5.0\,. \tag{2.7}$$

Using the expressions for bispectrum for Bogoliubov excited states given in Appendix A, for an approximately scale invariant β, we can compute the ratio of the bispectrum to the squared power spectrum (A.3) for a squeezed triangle of sides $\{k_s, k_s, k_l \ll k_s\}$ as

$$\frac{B_{\mathcal{R}}(k_s, k_s, k_l)}{P_{\mathcal{R}}(k_l), P_{\mathcal{R}}(k_s)} \sim |\beta(k_s)|\epsilon\frac{k_s}{k_l}\,. \tag{2.8}$$

For modes within the CMB observed range, the highest enhancement factor coming from the momentum ratio k_s/k_l is $\mathcal{O}\left(10^3\right)$[2], whereas based on our discussion β is at best of $\mathcal{O}\left(10^{-2}\right)$. Based on the present non-observation of tensor modes, we can approximately bound the slow-roll parameter ϵ during inflation to be also $\epsilon < \mathcal{O}\left(10^{-2}\right)$, which means the f_{NL} cannot be $\mathcal{O}\left(1\right)$ or larger. This leads us to conclude that when all the modes of the CMB are Bogoliubov excited, this does not lead to a non-gaussianity that can be observed by CMB measurements alone.

It is possible to consider the scenario where only some of the CMB modes are excited and not the others [12]. In this case, the procedure we used

[2]The actual enhancement factor in the calculation of f_{NL}^{local} will involve an integration over momenta and will be smaller. See, for example, [57]

to bound the excitation parameter β in Section 2.3 has to be done more carefully. The best way to weaken that argument would be to let the UV modes have a small (or even zero) β, therefore making the backreaction bound weaker (lowering β for the IR modes does not help weaken the bounds anyway). While this allows us to have a larger β for other (smaller) momenta, it is still necessary for this β to be small enough so as not to affect the approximate scale invariance of the CMB spectrum. Even for the lowest ℓ modes with large observational error bars on the power spectrum, it is not feasible to have $|\alpha + \beta|$ deviate from unity by more than a factor of 2, while for $\ell > 30$, the bounds are much stricter. Therefore, even discounting the backreaction bound, it may not be feasible for β to exceed $\mathcal{O}(0.1)$ for most CMB modes. Additionally, the amplitude (2.8) is proportional to $\beta(k_s)$, and therefore, lowering the highest momentum with a nonzero β also costs us on the momentum enhancement factor in the same proportion. Therefore, even in the case of a mixture of excited and unexcited modes, it is not possible to have large bispectrum amplitude in the squeezed limit and therefore the non-gaussianity must be small.

2.5 Implications for Pre-Inflationary Physics

An example of a physical mechanism that can produce Bogoliubov excited states was discussed in [32], which studied a transition from a pre-inflationary kinetic energy dominated era to an inflationary era. For extremely high momentum modes, the transition time may be large enough for the transition to be slow and adiabatic; however, for very low momentum modes with

characteristic time longer than the transition time, the transition must be sudden/non-adiabatic. For such modes, the transition amounts to a sudden change in the equation of state parameter w (which is the ratio of background pressure to background energy density), which activates the $\dot{\epsilon}/\epsilon$ term in (1.11) and generically leads to a different (non Bunch-Davies) mode function. For an almost-instantaneous transition, it was shown [32, 44] that the appropriate matching conditions for the mode function in the Heisenberg picture are given by

$$\begin{aligned} [\mathcal{R}]_{\pm} &= 0\,, \\ \left[\epsilon\dot{\mathcal{R}}\right]_{\pm} &= 0\,, \end{aligned} \tag{2.9}$$

with $[\,]_{\pm}$ indicating the difference between the values of the quantity within brackets evaluated before and after transition. The second condition indicates that any significant order of magnitude change in the slow roll parameter (which usually happens during transitions from non-inflationary phases into inflation, due to the small size of inflationary ϵ) could give rise to large amplitude of mode function after transition, and consequently a large excitation parameter β.

For the transition from kinetic energy domination to inflation, the excitation amplitude was calculated to be $|\beta|^2 \sim 3/(4\epsilon) \gg 1$. Since this magnitude far exceeds the bounds we obtained in Section 2.3, it is clear that such excited modes cannot comprise the observed CMB modes. This means that any such transition must have occurred sufficiently long before horizon exit of CMB

modes or must have been sufficiently slow so that modes that were significantly excited by the transition must be well outside horizon and well below the CMB momenta. The only window of possibility for such transitions to have a somewhat observable effect may be for the relatively less excited tail of the excited range of modes to correspond to the large error-bar low-ℓ CMB modes, while the fully excited modes lie completely outside the horizon [15]. Moreover, it is not clear whether such a scenario can be distinguished from other scenarios producing similar spectra.

2.6 Summary

In this chapter, we showed that Bogoliubov excited states can be very tightly constrained by using the sub-horizon and backreaction constraints simultaneously at early times (at the beginning of inflation or the time of excitation). One consequence of this tight constraint is that excited states cannot produce significant non-gaussianity in the squeezed/local limit that is observable through CMB measurements alone [12, 53]. Another consequence is that there are significant restrictions on imprints on the CMB spectrum from certain kinds of pre-inflationary physics, specifically a sudden transition from kinetic energy domination to inflation [32]; therefore if such transitions occurred in the early universe, they must have occurred early enough or slow enough so as not to affect the spectrum significantly [12, 15].

Chapter 3

Analyzing Multi-Field Tunneling Using Exact Bounce Solutions[1]

3.1 Introduction and Motivation

The string theory landscape motivates the study of multi-field potentials with a large number of metastable vacua [6, 19, 27, 41, 45, 51, 71, 75, 100, 103, 105]. Since our universe may have occupied a metastable vacuum in the past, for instance before inflation, or may do so today, it is of cosmological interest to study tunneling out of metastable vacua [25, 26, 54, 55, 67, 89, 96, 104, 109]. As the tunneling rate depends on the action of the bounce solution [38], computing the bounce action for various tunneling scenarios is of interest for studying tunneling transitions in the early universe.

A complete study of tunneling from the cosmological perspective must account for the effects of gravity [39] and finite temperature [88] on the tunneling process. However, obtaining the bounce solution and calculating its action for general multi-field potentials, a difficult problem to begin with, becomes considerably more complex where we account for these effects; therefore gravitational and finite temperature effects are often ignored in the interest of

[1]Portions of this chapter have been previously published in [11]

simplicity and we shall do the same in this chapter. Following this approach, Sarid [101] and later Greene et al. [64] discussed methods of estimating bounce action for quartic potentials using semi-numerical methods motivated by analytic arguments. Greene et al. [64] further concluded that for quartic potentials the bounce action decreases as a power law in the number of fields, agreeing with the lower bound calculated later in [14].

For multi-field potentials, part of the difficulty in calculating the bounce action arises from the difficulty in determining the appropriate tunneling trajectory. It is therefore reasonable to try and make the problem more manageable by splitting it into two smaller ones - determining the field-space trajectory of least action from the potential, and determining the bounce action along the least action trajectory. In this chapter, we discuss the second problem some detail.

Studying the dependence of the bounce action on the potential profile along the path would be facilitated by studying potentials with exact analytic bounce solutions. We present such a potential in the form of a binomial with non-integer powers which can be considered a generalization of the Fubini instanton potential [56, 88, 90]; unlike the standard Fubini instanton case, this potential has a barrier through which the field tunnels out. We also discuss a potential which has been previously known [52]. Through these examples of single field potentials with exact solutions, we study how barrier features are related to the bounce action. We see that a taller and wider barrier could lead to a smaller bounce action, contrary to what is expected from non-relativistic

quantum mechanics.

We then introduce a scaling argument that helps identify how the bounce action scales with barrier parameters for a general single field potential. We show how this is consistent with the results we have for the exactly solvable potentials. By extending this argument to additive multi-field potentials, we discuss the accuracy of the approximation scheme used by Greene et al. [64].

The rest of this chapter is organized as follows. In section 3.2, we briefly review tunneling in field theory. In section 3.3, we discuss special potentials for which an analytic bounce solution is available. In section 3.4, we introduce a scaling argument for bounce action of single field potentials and discuss its implications. In section 3.5, we apply this argument to gain insights on tunneling in multi-field potentials. In section 3.6, we conclude.

3.2 Review of Tunneling

In this section, we briefly review tunneling in field theory in a 4-dimensional Euclidean space in the absence of gravity, following the approach of Coleman in [38]. For the rest of this chapter, we always assume that the field(s) has (have) a metastable vacuum at the field-space origin $\vec{\phi} = \vec{0}$, with potential $V(\vec{0}) = 0$. We assume that this vacuum is surrounded on all sides by a barrier with $V > 0$. For tunneling to happen, there must exist regions beyond the barrier with $V < 0$ into which the field can tunnel.

For the case of a single field ϕ, it was proven in [40] that tunneling proceeds through the formation of an $O(4)$ symmetric bubble in Euclidean space (more specifically, it was shown that for a wide class of potentials, the action is minimized by $O(4)$ symmetric configurations). Therefore, the field value everywhere in space can be expressed as a function of the radius r measured from the center of the bubble. The field profile $\phi(r)$ obeys the following equation of motion obtained from assuming $O(4)$ symmetry [38]

$$\frac{d^2\phi}{dr^2} + \frac{3}{r}\frac{d\phi}{dr} = \frac{\partial V}{\partial \phi}\,, \quad \dot{\phi}(0) = 0\,, \quad \phi(\infty) = 0\,. \tag{3.1}$$

The solution to this equation $\bar{\phi}(r)$ (also called the bounce) corresponds to the position of a classical particle moving (in field space) in the inverted potential $-V(\phi)$ subject to time-dependent friction. The initial conditions impose that the particle starts at rest from the point where the field tunnels out ($\phi(0) = \phi_0$) and ends at rest at the false vacuum ($\phi(\infty) = 0$). The tunneling rate (per unit volume) is given by $\Gamma/V \sim A\, e^{-S/\hbar}$. Here S is the bounce action, which can be written as

$$\begin{aligned} S &= 2\,\pi^2 \int_0^\infty dr\, r^3 \left[\frac{1}{2}\left(\frac{d\bar{\phi}}{dr}\right)^2 + V(\bar{\phi})\right] \\ &= \frac{\pi^2}{2}\int_0^\infty dr\, r^3 \left(\frac{d\bar{\phi}}{dr}\right)^2 . \end{aligned} \tag{3.2}$$

Here, the last equality follows from Derrick's theorem [107].

For multi-field potentials, we are not aware of a proof for the $O(4)$ symmetry of the tunneling solution. However, $O(4)$ symmetry is generally

assumed [14, 64, 106] (though not always [19, 41, 92]), and we do the same here. Under this assumption, the story proceeds in a manner analogous to the single field case. Each field coordinate ϕ_i obeys the equation

$$\frac{d^2\phi_i}{dr^2} + \frac{3}{r}\frac{d\phi_i}{dr} = \frac{\partial V}{\partial \phi_i}\,, \quad \dot{\phi}_i(0) = 0\,, \quad \phi_i(\infty) = 0\,. \tag{3.3}$$

The solution to this set of equations is analogous to the position vector $\vec{\phi}$ of a particle moving subject to friction in an inverted multi-dimensional potential $-V(\vec{\phi})$ along some specific trajectory. Since the position, velocity and acceleration are multi-component vectors, we can reorganize these equations into a more intuitive form by separating the components parallel to and perpendicular to the trajectory of the particle (see, for example, [106]). We begin by parametrizing points on the trajectory in terms of the field-space distance from the false vacuum measured *along the trajectory*[2], $\phi(r)$. In terms of this variable, the equations (3.3) can be re-written as

$$\begin{aligned} \frac{d^2\phi}{dr^2} + \frac{3}{r}\frac{d\phi}{dr} &= \frac{\partial}{\partial\phi}V(\vec{\phi})\,, \\ \frac{d^2\vec{\phi}}{d\phi^2}\left(\frac{d\phi}{dr}\right)^2 &= \nabla_\perp V(\vec{\phi})\,. \end{aligned} \tag{3.4}$$

Here, $\frac{\partial}{\partial\phi}V(\vec{\phi})$ and $\nabla_\perp V(\vec{\phi})$ refer to the tangential and perpendicular components of the gradient of the potential respectively. The first equation is similar

[2]Note that $\phi(r)$ is the arc-length along the trajectory, and *not* the radial distance from the field-space origin. At any point on the trajectory $d\phi^2 = \sum_{i=1}^{N} d\phi_i^2$, but in general $\phi^2(r) \neq \sum_{i=1}^{N} \phi_i^2(r)$.

to the single field equation of motion (3.1), while the second equation causes the bounce trajectory to curve (in field-space) when the potential slopes in the transverse directions. If the trajectory is known, the multi-field problem can be treated effectively as a single field problem with a field ϕ subject to a potential $V(\phi)$ (the "potential profile" on the trajectory), with an action identical in form to (3.2).

If there are multiple solutions to (3.4), the one with the lowest action (the bounce) typically dominates tunneling. For a general potential profile, it is possible to get a rough estimate/underestimate of the action [14, 64] after truncating the integral[3] in (3.2)

$$\begin{aligned} S &\gtrsim r_\Sigma^3 \frac{\pi^2}{2} \int_{r_\Sigma}^{\infty} dr \left(\frac{d\phi}{dr}\right)^2 \\ &\gtrsim r_\Sigma^3 \frac{\pi^2}{2} \int_0^{\phi_\Sigma} d\phi \sqrt{2\,V(\phi)} \\ &\approx r_\Sigma^3\, \pi^2 \int_0^{\phi_S} d\phi \sqrt{2\,V(\phi)}\,. \end{aligned} \tag{3.5}$$

Here, r_Σ and ϕ_Σ refer to the values of r and ϕ at the point on the trajectory where the potential is equal to its false-vacuum value (if there are multiple such points, we take the one closest to the false vacuum on the trajectory). Similarly, ϕ_S refers to the value of ϕ at the local maximum of the potential profile closest to the false vacuum.

[3]The truncated integral $\int_0^{\phi_\Sigma} d\phi\sqrt{2V(\phi)}$ is commonly referred to as "surface tension".

In [64], the authors write the pre-factor multiplying the surface tension integral in terms of the bounce radius r. Since bounce radius is not a well-defined quantity in general (except in the case of a thin-wall bubble), we shall define it to be r_Σ. As a simplifying assumption, they also argued that tunneling occurs through a nearby saddle point which presents the smallest barrier. When that happens, our definition of ϕ_S would correspond to the location of this saddle point. However, we note that the bounce trajectory in general does not have to pass through a saddle point [80].

3.3 Single Field Potentials With Exact Bounce Solutions

In this section, we discuss two single field potentials with exact analytical solutions to (3.1).

3.3.1 Binomial Potential With Non-Integer Powers

The first example we discuss can be considered a generalization of the Fubini instanton to non-integer powers. The potential is

$$V(\phi) = \frac{4\,u\,n^2(n-1)}{2\,n+1}\phi^{(2n+1)/n} - 2\,u\,v\,n^2\phi^{(2n+2)/n}, \tag{3.6}$$

where $\{u, v, n\} \in \mathbb{R}$ with $u > 0$, $v > 0$ and $n > 1$.

The exact bounce solution and bounce action for this potential are

given by

$$\bar{\phi}(r) = \frac{1}{(u\,r^2+v)^n}\,,$$

$$S\left[\bar{\phi}\right] = \frac{n\,\pi^2}{(4\,n^2-1)}\frac{1}{u\,v^{2n-1}}\,. \tag{3.7}$$

Unlike the standard Fubini case, this potential has a minimum at $\phi = 0$ followed by a barrier for small values of ϕ and a runoff (to $-\infty$) for large values of ϕ. In general, this potential represents a case of thick-wall tunneling.

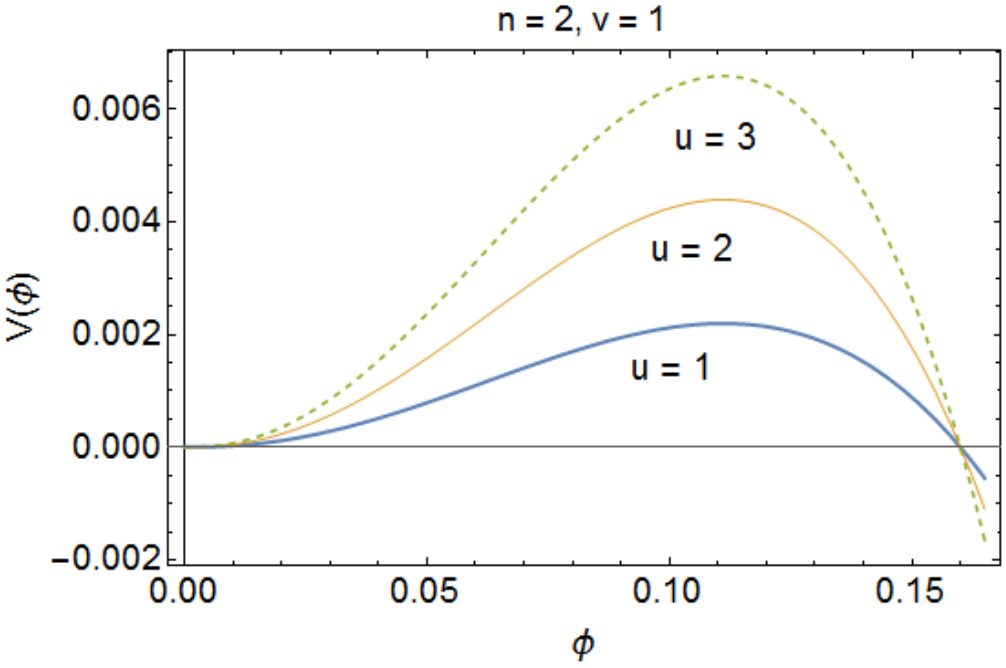

Figure 3.1: Binomial potential scaling with u.

For physical theories, we might worry about the runoff and also about the behavior of the potential for $\phi < 0$. The former could be addressed by adding terms that avoid runoff for large values of ϕ, and the latter by replacing

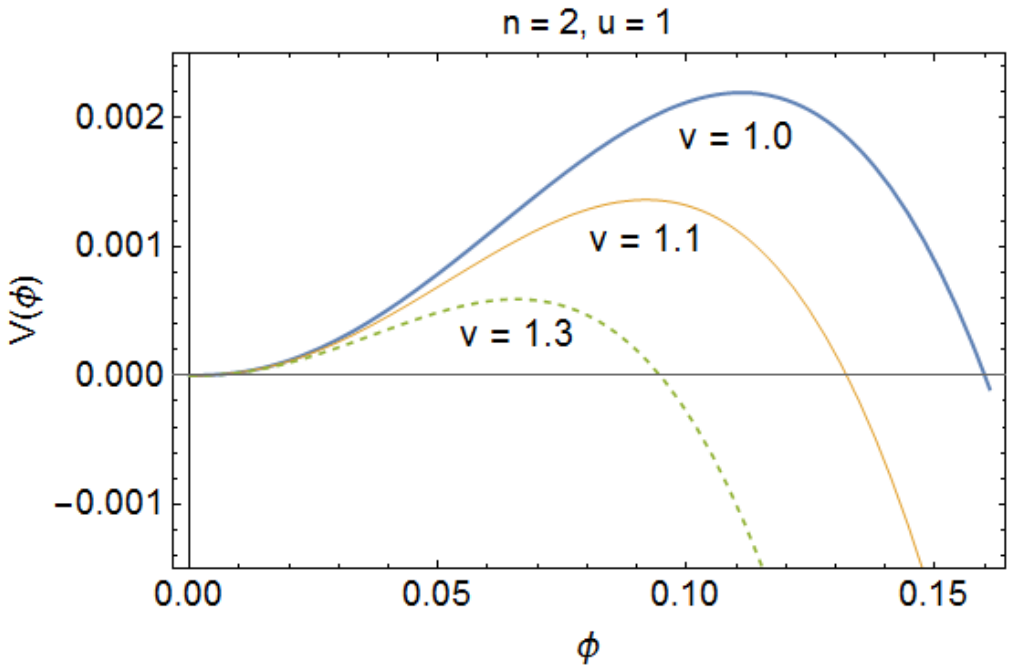

Figure 3.2: Binomial potential scaling with v.

ϕ with $|\phi|$. The bounce itself cares only about the potential profile along the tunneling trajectory (between $\phi = 0$ and $\phi = 1/v^n$), not beyond it.

We notice that for $0 < n \leq 1$ the potential (3.6) is well defined, but it does not have a barrier. Therefore the solution does not involve tunneling. For $n = 1$ we recover the Fubini case. This can be compared to the potential in equation (4.1) of [88] in the zero-temperature limit with $M = 0$. In that limit, on identifying $\lambda = 8\,u\,v$ and $\rho^2 = v/u$ we see that the bounce solution in equation (4.3) of [88] is identical to our bounce solution (3.7).

For larger integer values of n, the potential (3.6) involves fractional powers and bears some resemblance to potentials encountered in the string

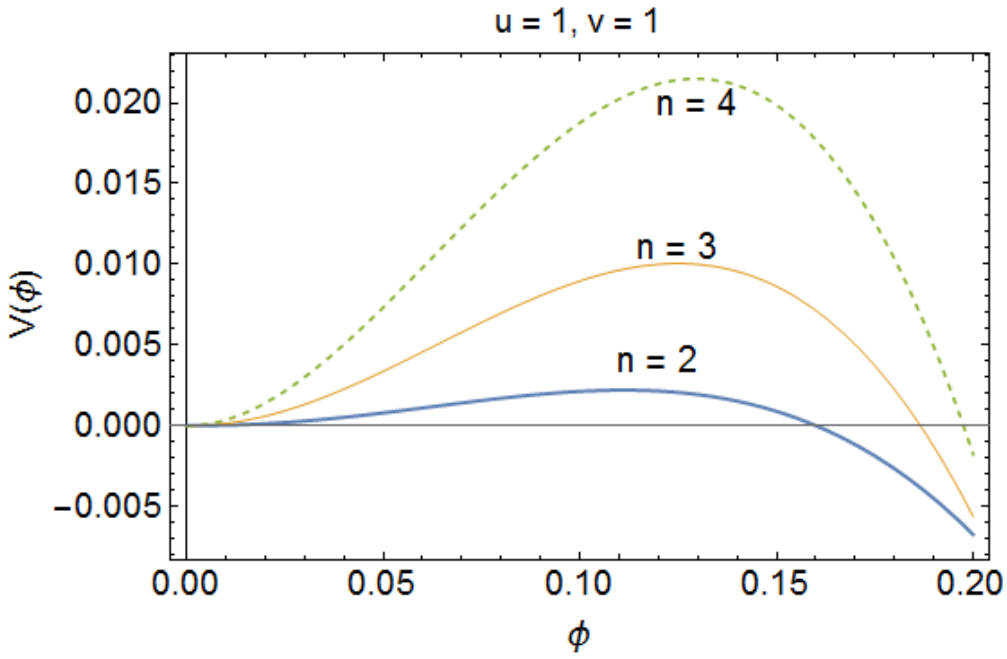

Figure 3.3: Binomial potential dependence on n.

theory landscape [103]. It is worth investigating whether potentials with exactly this form - a binomial with two non-integer powers between 2 and 4 - appear somewhere in physically well motivated models.

We note that increasing the value of the parameter u corresponds to scaling up the potential, while increasing v corresponds to scaling down the potential *as well as* making the barrier narrower as seen in Figs. 3.1 and 3.2. Both of these changes tend to bring down the bounce action. If we fix u and v and vary the parameter n, the dependence is more complicated. To take a special case, if we fix $v = 1$, we see that as we increase n, the barrier width and the barrier height increases (the width asymptotes to a constant) while the bounce action decreases, as shown in Fig. 3.4. Hence, a higher

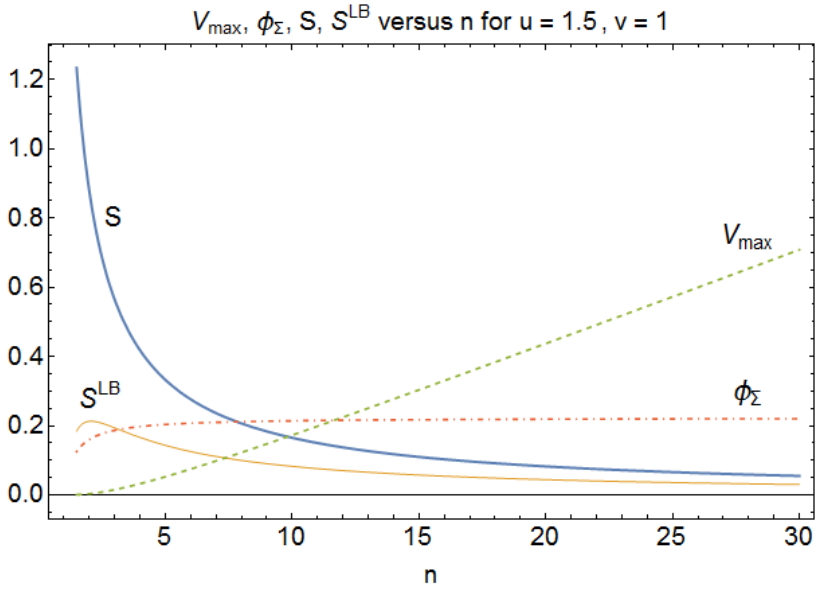

Figure 3.4: Scaling of various quantities with n for the binomial potential (3.6) with $u = 1.5$, $v = 1$. The four lines represent action S (thick, blue), approximation S^{LB} (thin, orange), height of the potential peak V_{max} (dashed, green) and barrier width ϕ_Σ (dot-dashed, red). S^{LB} scaled up by a factor of 5 for ease of comparison.

barrier can result in a lower action, as known from scaling relations [107]. The dependence of bounce action on scaling of barrier parameters will be studied in greater generality in section 3.4.

3.3.2 Logarithmic Potential

We now discuss a previously known [52] potential with exact bounce solution.

$$V(\phi) \;=\; \frac{1}{2}m^2\phi^2\left[1-\ln\left(\frac{\phi^2}{w^2}\right)\right]\,, \quad \{m,w\}\in\mathbb{R}\,. \tag{3.8}$$

The bounce solution is given by

$$\bar{\phi}(r) = w \exp\left[-\frac{1}{2}m^2 r^2 + 2\right],$$

$$S = \frac{\pi^2 e^4}{2}\frac{w^2}{m^2}. \tag{3.9}$$

Similar to the binomial potential, this potential has a barrier near the false vacuum followed by a run-off for large values of ϕ. The log function has a singularity at $\phi = 0$, but the potential has a well defined limit at that point. Scaling the parameters w and m correspond to scaling the field-space width of the barrier or scaling the height of the potential (with corresponding changes to the radius-scale r_Σ). How the bounce action depends on these parameters is also clear; the bounce action decreases with the barrier height and increases with the barrier width. We shall generalize this discussion in the next section.

3.4 Scaling of Bounce Action With Potential Profile

3.4.1 Scaling Argument

In this section we shall discuss how the scaling of the potential profile along the bounce trajectory (which changes the height and width of the barrier) affects the bounce action. Since this is effectively a single field problem, we shall call the field variable ϕ, corresponding to either the single field coordinate (for the single field potential) or the arc length along a multi-field trajectory (for the multi-field potential). The potential profile along the trajectory includes the barrier region ($V > 0$) and also the region beyond it ($V < 0$).

Let us start with a tunneling potential $V(\phi)$ with a bounce solution $\bar{\phi}(r)$ (not necessarily analytic). In order to parametrize scaling, we introduce a variable $g > 0$, with $g = 1$ corresponding to the original potential. On changing the value of g, let the potential V (barrier height) and the length-scale in field-space ϕ (barrier width) scale as powers of g, g^a and g^b respectively. We denote the rescaled potential and bounce solution as V_g and $\bar{\phi}_g$ respectively ($V_1 \equiv V$ and $\bar{\phi}_1 \equiv \bar{\phi}$). We observe that for the scaling to be consistent, the typical radius r must also scale. Collectively, the scaling relations are as follows

$$\begin{aligned} r_g &\equiv g^c\, r\,, \\ \phi_g &\equiv g^b\, \phi\,, \\ \bar{\phi}_g(r_g) &= g^b\, \bar{\phi}(r)\,, \\ V_g(\phi_g) &= g^a\, V(\phi)\,. \end{aligned} \tag{3.10}$$

In order to ensure that $\bar{\phi}_g$ satisfies the equation of motion (3.1), we must have an additional constraint

$$2\,c \;=\; 2\,b - a\,. \tag{3.11}$$

This is consistent with the scaling argument presented in [102] for the single-field case. From the scaling relations (3.10) and (3.11) and from (3.2), the bounce action scaling is obtained

$$S_g = g^{4b-a} S\,. \tag{3.12}$$

We may also check the scaling of the approximation/lower bound (3.5). Naming this quantity as S^{LB}, we observe that it scales as $S^{LB}_g = g^{4b-a} S^{LB}$,

which is the same as the bounce action. Therefore, *any change* in the potential profile and the bounce solution, provided it can be reduced to a scaling of the height of the potential profile and/or the field space length scale will maintain the level of accuracy of the approximation. Changes to the shape of the potential profile (which cannot be reduced to some form of scaling) can, however, affect the accuracy of the approximation (3.5).

3.4.2 Application to Exact Solutions

Let us now apply the scaling argument for the potentials discussed in section 3.3. For the logarithmic potential (3.8), if the parameters scale as $w_g = g^\gamma w$ and $m_g = g^\delta m$, ϕ and r can be rescaled as

$$\begin{aligned} r_g &\equiv g^{-\delta} r \,, \\ \phi_g &\equiv g^\gamma \phi \,, \end{aligned}$$

to obtain

$$\begin{aligned} \bar{\phi}_g(r_g) &= g^\gamma w \exp\left[-\frac{1}{2} g^{2\delta} m^2 r_g^2 + 2\right] = g^\gamma \bar{\phi}(r) \,, \\ V_g(\phi_g) &= \frac{1}{2} g^{2\delta} m^2 \phi_g^2 \left(1 - \ln \frac{\phi_g^2}{g^{2\gamma} w^2}\right) = g^{2(\gamma+\delta)} V(\phi) \,. \end{aligned} \tag{3.13}$$

This gives us all the scaling exponents in (3.10) and (3.12). This same approach can be followed for the binomial potential. The results are summarized in Table 3.1.

Potential	Transform	V-scaling	ϕ-scaling	r-scaling	Action-scaling
		a	b	c	
Binomial	$u_g = g^{\alpha} u$ $v_g = g^{\beta} v$	$\alpha - (2n+1)\beta$	$-n\beta$	$(\beta - \alpha)/2$	$S_g = g^{-\alpha-(2n-1)\beta} S$
Log	$w_g = g^{\gamma} w$ $m_g = g^{\delta} m$	$2(\gamma + \delta)$	γ	$-\delta$	$S_g = g^{2(\gamma-\delta)} S$

Table 3.1: Summary of scaling relations for the binomial (3.6) and logarithmic (3.8) potentials.

We note that the g-scaling of the action in Table 3.1 agrees with the exact expressions (3.7) and (3.9) if we plug in the scaling of parameters u, v, w and m. This indicates consistency of the scaling approach.

3.4.3 Implications of the Scaling Argument

We shall now discuss the insights gained from the scaling argument regarding the relation between the barrier parameters and the bounce action. We begin by noting that the bounce action scales as g^{4b-a}. This means that in general, taller ($a > 0$) and narrower ($b < 0$) barriers lead to a smaller bounce action. In fact, it is possible to make the barrier larger in all respects (increase in both height and width) and still reduce the bounce action provided the barrier height increases fast enough ($a > 4b$) to compensate for the increase in width. The reason for this becomes clear by recalling the estimate (3.5): the action decreases because the decrease in r_Σ^3 is faster than the increase in the surface tension integral.

We note that this is different from the case of non-relativistic quantum

mechanics, where barriers with larger surface tension always lead to a larger action in the absence of the r^3 factor[4]. Therefore, in the case of multi-field potentials, we cannot assume tunneling happens in the direction of the "smallest" barrier. In section 3.5, using additive potentials, we explicitly show situations where the tunneling trajectory lies in the direction of a larger barrier.

While the scaling argument captures the dependence of action on two barrier parameters (height and width), the actual diversity in the types of potential profiles is far greater than what can be described using only two parameters. Changing the value of n in the binomial potential (3.6) provides one such example that leads to a non-scaling change in shape of the profile, as seen in Fig. 3.3. The dependence of barrier parameters and bounce action on n can be seen in Fig. 3.4. It can be clearly seen that for small values of n, the exact bounce action S and the approximation S^{LB} scale differently. We note that for $n \gg 1$, changing n reduces to a scaling of the potential, which explains why these curves scale the same way for large values of n.

3.5 Application to Multi-Field Potentials

3.5.1 Additive Potentials

One of the simplest ways of going from a single field potential to an N-field potential is by defining an additive potential

$$V\left(\vec{\phi}\right) = V\left(\phi_1, \phi_2, ...\phi_N\right) = \sum_{i=1}^{N} V_i\left(\phi_i\right) \ . \tag{3.14}$$

[4]The surface tension in both cases scales as $\sigma_g = g^{(a+2b)/2}\sigma$.

Owing to the fact that the different field coordinates ϕ_i behave as independent, uncoupled fields, the N equations (3.3) completely decouple to give N independent single field equations of motion of the type (3.1).

For simplicity, let us assume that each of the V_i's has a non-trivial tunneling solution $\bar{\phi}_i(r)$ apart from the trivial one ($\phi_i(r) = 0$). This means that the there are $2^N - 1$ solutions for the N-field bounce, corresponding to each field picking either the trivial or non-trivial solution[5].

For additive potentials, the action for N-fields is obtained by adding the single field action for each of the N fields (3.2) which are completely independent of each-other

$$S = \sum_{i=1}^{N} \int_0^\infty dr\, r^3 \left[\frac{1}{2} \left(\frac{d\phi_i}{dr} \right)^2 + V_i \left(\phi_i(r) \right) \right] = \sum_{i=1}^{N} S_i \,. \tag{3.15}$$

Since each of the S_i's can be either positive or 0, the lowest action is provided by the solution where one of the S_i's takes the smallest non-trivial value and all others are 0; this is the bounce action.

Effectively, tunneling happens along (or is dominated by) a field axis which corresponds to the V_i that minimizes the bounce action among the N choices available. This does *not* have to correspond to the axis with the smallest barrier. For example, let us consider an N-field potential where each of the V_i's is a binomial potential (3.6) with the same value of n but with different u and v (which scale as powers of g, with a different g for each axis).

[5]We discount the solution $\phi_i(r) = 0 \; \forall \, i$ which does not involve tunneling out of the false vacuum.

If the exponents in Table 3.1 are such that $\{\alpha > 0, \beta < 0\}$ and $\alpha > (2n-1)|\beta|$, the axis corresponding to highest value of g would dominate tunneling. This is not the direction with the smallest barrier as all of the other field axes have shorter and narrower barriers.

3.5.2 N-Dependence

We may study the dependence of the bounce action on the number of fields N to see how N affects vacuum metastability. The answer will depend on what class of additive potentials we consider, i.e., what restrictions we put on them. Let us consider building an N-field additive potential of the form (3.14), starting from individual single field components $V_i(\phi_i)$. For simplicity, we assume the V_i's are all potentials of the same type (for example, potentials such as (3.6) or (3.8)) differing only in the choice of parameters (such as u, v, m or w), which could all be selected from random distributions. By this (very restrictive) choice, we are requiring that the potential profile along each of the axes will have the same shape (but can have different scaling).

We shall try to enforce some measure of N-independence in the potential that we construct by requiring that for any N, the typical values of the potential (heights of its peaks and valleys) at *typical points* on the unit $N-1$ sphere in field-space must be N-independent. This constraint is inspired by a similar approach in [64] for the case of quartic potentials. Points on the unit sphere can be parametrized as $\vec{\phi} = \frac{1}{\sqrt{N}}(c_1, c_2, ..., c_N)$, where each of the c_i's

are typically $O(1)$[6].

Since the potential is additive, we require each component potential $V_i(c_i/\sqrt{N})$ to scale as $1/N$, so that the overall potential (at *typical* points) does not scale with N. Therefore, by imposing this particular form of N-independence in the potential, we are forced to choose parameters (u, v, etc.) from distributions such that the V_i's and the length-scales of the ϕ_i axes scale with N.

From the arguments in the preceding section, we know that tunneling happens along a field axis (the one which minimizes the action). Therefore, the barrier height and barrier width on the *tunneling trajectory* also scale as $1/N$ and $1/\sqrt{N}$, respectively (due to the fact that a field axis is *not* a typical direction). Here N plays the role of g in our scaling arguments, and we are left with the scaling exponents $a = -1/2$ and $b = -1$. This automatically fixes $c = 0$, i.e., the typical bounce radius is N-independent. The exact bounce action (3.2) scales as N^{-1}, and so does the approximation (3.5). Thus, for these potentials, tunneling probability is enhanced as N grows. This agrees with the result found in [64] where the action scales as $N^{-\alpha}$ with $\alpha > 1$.

3.5.3 Multi-Field Potentials With Cross Couplings

In the case of additive potentials, the bounce solution satisfies the longitudinal equation of (3.4) because it is effectively a single field bounce. The

[6]Points on the unit-sphere also satisfy $\sum_{i=1}^{N} c_i^2 = N$.

transverse equation is trivially satisfied because the path is a straight line and the variation of the potential in all the remaining $N-1$ directions is also 0 (all the remaining field coordinates rest at a minimum of their potential)[7].

When we move away from additive potentials to potentials with cross-couplings, the story becomes considerably more complicated. For such potentials, straight line directions with no transverse gradients do not generally exist which makes it difficult to identify solutions that satisfy both equations (3.4). However, if we are able to identify the bounce trajectory, it is possible to compute either the exact action (3.2) or its approximation (3.5), both of which scale the same way.

Greene et al. [64] sought to make the multi-field tunneling problem tractable for quartic potentials by calculating estimate (3.5) in two steps. In one step, they assumed that the potential profile of the trajectory corresponds approximately to a straight-line path and studied the variation of the bubble radius (presumably r_Σ or something similar) for quartic potential profiles. They observed that the radius usually took on values within the same order of magnitude for a distribution of sampled potentials and therefore attributed a standardized value of radius for their bounce action estimate. In the second step, they calculated the surface tension integral for the most "obvious" choice of tunneling trajectory, the one passing through the smallest surface tension barrier. Our arguments indicate that this step is not justified as it may pick

[7]Note that for the non-axis solutions to (3.3), the LHS and RHS of the second equation are typically nonzero.

the wrong tunneling direction/trajectory.

Using a code improvised from [106], we computed the exact action for two-field potentials in order to compare with the estimate of Greene et al. [64]. For the potentials we considered, their estimate was of the same order of magnitude as the exact bounce action. It would be interesting to check the approximation for larger numbers of fields by numerically computing the bounce action to see if the approximation still agrees.

3.6 Conclusions

We introduced a new class of potentials with exact analytic bounce solutions corresponding to tunneling through a barrier in the absence of gravity. These solutions could be considered a generalization of the Fubini instanton to non-integer powers and could prove to be valuable for further study as they may possibly have a role to play in the string theory landscape.

We used scaling arguments to observe that for tunneling potentials with some fixed shape of the potential profile, the following hold true:

1. Making the barrier taller ($a > 0$) and narrower ($b < 0$) always lowers the bounce action.

2. Making the barrier taller ($a > 0$) and broader ($b > 0$) can still lead to a lower bounce action if the height increases faster than the width to the fourth power ($a > 4b$).

Furthermore, we recognize that scaling does not account for the considerable diversity in shapes of barriers, which means that the dependence of action (and bounce radius) on various shapes of potential profiles is still an open and rich problem in its own right.

We also observe that the approximation (3.5), which involves multiplying the "surface tension" of the bubble by its 3-dimensional surface area, scales with barrier parameters the same way as the bounce action; therefore, its accuracy will be preserved under any transformation that could be described purely in terms of scaling.

Finally, we note that the intuition from single field potentials directly translates to the case of additive multi-field potentials, where the bounce trajectory lies along one of the field axes. For general multi-field potentials, identifying the actual bounce trajectory is still an open problem and we do not yet have a simple way of calculating or estimating the bounce trajectory corresponding to tunneling out of a false vacuum.

Chapter 4

Higgs Portal to Inflation and Fermionic Dark Matter[1]

4.1 Introduction

The paradigm of cosmic inflation is uniquely interesting from both the quantum gravity as well as the particle phenomenology viewpoints. While the simple single-field slow roll scenario is consistent with observations, this picture cannot be considered completely satisfactory until the connection between the inflaton field and the more familiar standard model fields is established. A potentially strong connection between inflation and particle phenomenology was pointed out a few years ago when it was shown that the standard model Higgs (albeit with a nonminimal coupling to gravity) could perform the role of the inflaton [24]. While the inflationary predictions of this simple model are still within the observationally allowed region [2], there are significant question marks on its viability.

One important concern is the instability of the Higgs potential in Higgs inflation. For the currently measured values of Higgs mass ($m_h \approx 125$ GeV) and the top quark mass ($m_t \approx 173$ GeV), the Higgs self-coupling runs to

[1]Portions of this chapter have been previously published in [16]

negative values well below the Planck scale or the inflationary scale (which is $\mathcal{O}(10^{17})$ GeV) [43]. Without new physics, this can only be avoided by assuming the top quark pole mass is about 3σ below its central value [99]; even so, the inflationary predictions could potentially be sensitive to the exact values of these parameters [8].

Another concern regarding Higgs inflation is whether the large non-minimal coupling parameter ($\xi \sim \mathcal{O}(10^4)$) in this theory would affect unitarity [20, 23, 28, 29, 31, 72, 84, 85, 97]. Graviton exchange in WW scattering causes tree-level unitarity violation at the energy $M_{\rm pl}/\xi$. This energy is lower than the scale of the Higgs field during inflation $M_{\rm pl}/\sqrt{\xi}$, and is comparable to the inflationary Hubble rate. If this is true, new particles and interactions should be introduced at the scale $M_{\rm pl}/\xi$ to restore unitarity. The new physics will modify the Higgs potential above the scale $M_{\rm pl}/\xi$ and thus make the predictions of Higgs inflation unreliable. It was recently suggested [31] that if we consider loop corrections at all orders unitarity may be restored. While there has been some debate on this topic [20, 23, 28, 29, 31, 72, 84, 85, 97], we will not be addressing this issue here.

In recent years, many extensions to the standard Higgs inflation model have been discussed [10, 33, 59, 60, 69, 70, 93, 94]. Additionally, there have been many efforts to connect Higgs inflation to the dark matter paradigm [17, 37, 42, 62, 68, 74, 77, 78, 83, 86, 95, 110]. In particular, there have been attempts at constructing Higgs-portal type models [62, 74, 78], where dark matter is coupled to the standard model through the Higgs field.

In this chapter, we study a scalar portal model involving a singlet fermionic dark matter field and a singlet scalar coupled to the Higgs which functions as the portal. Our primary motivation is to investigate the possibility of stabilizing the Higgs potential (or the scalar potential) using mixing between the two scalars. Through this, we seek to avoid having to fine-tune the top quark mass in order to save the inflation model. Unlike the Higgs portal models in Ref. [62, 78], the dark matter is fermionic and thus prevents the potential perturbativity problem in the singlet scalar potential.

An added attraction of this model is phenomenological connection between the inflationary paradigm with the dark matter paradigm. Similar models have been studied in the context of dark matter phenomenology in the past [50, 61, 79, 87, 98], but their relevance in the context of inflation has not been studied before. We consider inflation driven by either the Higgs field or the singlet scalar field which is nonminimally coupled to gravity. Reheating proceeds in the usual manner producing thermal dark matter. We explore the parameter region that produces the correct relic abundance of dark matter and is also consistent with direct detection and collider constraints, apart from providing successful inflation.

The chapter is organized as follows. In Section 4.2, we introduce our model. In Section 4.3, we discuss the mechanism of inflation and calculation of inflationary parameters. In Section 4.4, we discuss the phenomenological constraints we have used for constraining the parameter space of our model. In Sections 4.5 and 4.6, we discuss our numerical results and conclusions.

4.2 The Model

Our model consists of an extension of the standard model with the addition of a gauge singlet fermionic dark matter ψ and a gauge singlet scalar S to the standard model content. Here we assume the dark matter ψ consists of two Weyl components ψ_1 and ψ_2. We impose a Z_2 symmetry on the model under the action of which S and ψ_1 are odd while ψ_2 and all the SM particles are even. In other words, under the Z_2 action, we have $\psi \to \gamma^5\psi$. The Z_2 symmetry simplifies the model by eliminating odd power terms in the scalar potential while at the same time allowing the Yukawa coupling $y_\psi S\bar{\psi}\psi$ that induces a mass for the dark matter at non-zero expectation value for S.

The relevant Jordan frame Lagrangian for the model can be written as

$$\begin{aligned}\mathcal{L} &= \sqrt{-g}\Bigg[-\frac{1}{2}R\left(M_{\rm pl}^2 + 2\xi_h H^\dagger H + \xi_s S^2\right) \\ &\qquad +\partial_\mu H^\dagger \partial^\mu H + \frac{1}{2}(\partial_\mu S)^2 - V(H,S) + \mathcal{L}_{\rm DM}\Bigg], \quad (4.1)\end{aligned}$$

where $M_{\rm pl}$ is the reduced Planck mass and $H = \begin{pmatrix} \pi^+ \\ \frac{1}{\sqrt{2}}(\phi + i\pi^0) \end{pmatrix}$ is the Higgs doublet.

The tree-level two-field scalar potential is

$$\begin{aligned}V(H,S) = &-\mu_h^2 H^\dagger H + \lambda_h (H^\dagger H)^2 - \frac{1}{2}\mu_s^2 S^2 + \frac{1}{4}\lambda_s S^4 \\ &+ \frac{1}{2}\lambda_{sh} H^\dagger H S^2 + \kappa S. \end{aligned} \quad (4.2)$$

The soft Z_2 breaking coefficient κ is very small and only serves to raise the degeneracy of the Z_2 symmetry to avoid domain wall problem. In the rest

of our discussion we shall omit this term. The connection between the Higgs boson and dark matter is through the real scalar S. The fermion dark matter lagrangian is given by

$$\mathcal{L}_{\rm DM} = i\bar{\psi}\gamma^\mu\partial_\mu\psi - y_\psi S\bar{\psi}\psi. \tag{4.3}$$

Note that due to the Z_2 symmetry, no Dirac mass is allowed for ψ.

After symmetry breaking, in general, both S and ϕ (the neutral component Higgs doublet H) in the tree-level potential develop vacuum expectation values, denoted as

$$v \equiv \langle\phi\rangle, \quad u \equiv \langle S\rangle. \tag{4.4}$$

The minimization conditions on the first derivative of the tree-level potential allows us to write the second derivatives of the tree-level potential as a squared mass matrix of ϕ and S:

$$\begin{aligned}\mathcal{M}^2(\phi,S) &\equiv \begin{pmatrix} m^2_{\phi\phi} & m^2_{s\phi} \\ m^2_{s\phi} & m^2_{ss} \end{pmatrix} \\ &= \begin{pmatrix} \lambda_h(3\phi^2 - v^2) + \frac{\lambda_{sh}}{2}(S^2 - u^2) & \lambda_{sh}\phi S \\ \lambda_{sh}\phi S & \lambda_s(3S^2 - u^2) + \frac{\lambda_{sh}}{2}(\phi^2 - v^2) \end{pmatrix}.\end{aligned} \tag{4.5}$$

Diagonalizing the above matrix, we can relate the mass squared eigenvalues m_h^2 and m_s^2 (with $m_s > m_h$) in terms of these parameters and write the eigenvectors (corresponding to the "Higgs" and "scalar" directions, denoted by h and s) as

$$\begin{pmatrix} h \\ s \end{pmatrix} = \begin{pmatrix} \cos\tilde{\varphi}(\phi,S) & \sin\tilde{\varphi}(\phi,S) \\ -\sin\tilde{\varphi}(\phi,S) & \cos\tilde{\varphi}(\phi,S) \end{pmatrix} \begin{pmatrix} \phi \\ S \end{pmatrix}, \tag{4.6}$$

where the mixing angle $\tilde{\varphi}(\phi, S)$ is given by

$$\tan 2\tilde{\varphi}(\phi, S) = \frac{2m_{s\phi}^2}{m_{ss}^2 - m_{\phi\phi}^2}\,. \tag{4.7}$$

We define the mixing angle today as

$$\varphi \equiv \tilde{\varphi}(v, u) = \frac{1}{2}\arctan\frac{\lambda_{sh} v u}{\lambda_s u^2 - \lambda_h v^2} \tag{4.8}$$

In this chapter, we shall consider inflation starting either on the ϕ-axis or the S-axis, which means that either ϕ or S would take large field values (typically $\mathcal{O}(10^{14}\,\mathrm{GeV})$ or higher) while the other field would take much smaller value (typically, $\mathcal{O}(1\,\mathrm{TeV})$ or smaller). In both cases, it is easy to see that the mixing is very small ($\tilde{\varphi}(\phi, S) \sim 0$) and therefore it is appropriate to describe this as inflation along the Higgs direction ($h-$inflation) or inflation along the scalar singlet direction ($s-$inflation).

4.3 Inflation

4.3.1 $h-$Inflation

This is a variant of the standard Higgs inflation scenario with the Higgs potential modified by interactions between the Higgs field and the scalar s. We begin by using as input parameters the scalar mass m_s, mixing angle φ, the quartic interaction coefficient λ_{sh} and the dark matter Yukawa coupling y_ψ at the electroweak scale. By requiring the eigenvalues of the mass matrix (4.6) to be $m_h = 125.7\,\mathrm{GeV}$ and m_s, we can obtain the scalar vev at low energies (u) and also the values of the self interactions λ_h and λ_s at the electroweak

scale. The value of ξ_h is determined by requiring the appropriate normalization of curvature perturbations during inflation and is therefore not an input parameter. In the case of standard (tree level) Higgs inflation, a large value $\xi \sim \mathcal{O}\left(10^4\right)$ is necessary to match the observed amplitude of fluctuations (Eq.(4.15)).

The non-minimal coupling with gravity is usually dealt with by transferring the Lagrangian to the Einstein frame by performing a conformal transformation. But before doing so, it is necessary to determine how to impose quantum corrections to the potential [47, 48]. There are two approaches in general: one is to calculate the quantum corrections in the Jordan frame before performing the conformal transformation; the other is to impose quantum corrections after transferring to the Einstein frame. The two approaches give slightly different results [8], and we adopt the first one. The running values of various couplings from electroweak scale to the planck scale in the Jordan frame can be obtained using the renormalization group equations given in Appendix B. The running behavior of couplings for a typical data point is shown in Fig. 4.1.

The quantum corrected effective Jordan frame Higgs potential (the two-field potential evaluated along the Higgs axis) at large field values (h) can be written as

$$V(h) = \frac{1}{4}\lambda_h(\mu)h^4\,, \tag{4.9}$$

where the scale can be defined to be $\mu \sim \mathcal{O}(h) \approx h$ in order to suppress the quantum correction.

Following the usual procedure (outlined in Appendix C), we get to the Einstein frame by locally rescaling the metric by a factor Ω^2, which in our case is given by $\Omega^2 = 1 + (\xi_h h^2 + \xi_s s^2)/M_{\rm pl}^2 \approx 1 + \xi_h h^2/M_{\rm pl}^2$, the ξ_s term neglected because we are on the h-axis with $s \sim 0$. This leads to a non-canonical kinetic term for h, which can be resolved by rewriting the inflationary action in terms of the canonically normalized field χ as

$$S_{\rm inf} = \int d^4x \sqrt{\tilde{g}} \left[\frac{M_{\rm pl}^2}{2} R + \frac{1}{2} (\partial\chi)^2 - U(\chi) \right] \tag{4.10}$$

with potential

$$U(\chi) = \frac{\lambda_h \left(h(\chi)\right)^4}{4\Omega^4} \tag{4.11}$$

where the new field χ is defined by

$$\frac{d\chi}{dh} = \sqrt{\frac{3M_{\rm pl}^2 \left(d\Omega^2/dh\right)^2}{2\Omega^4} + \frac{1}{\Omega^2}} \approx \sqrt{\frac{1 + \xi_h h^2/M_{\rm pl}^2 + 6\xi_h^2 h^2/M_{\rm pl}^2}{\left(1 + \xi_h h^2/M_{\rm pl}^2\right)^2}} \,. \tag{4.12}$$

Note that λ_h and ξ_h have a scale (h) dependence. The potential $U(\chi)$ for a typical data point for $h-$inflation is shown in Fig. 4.1.

From the inflationary potential $U(\chi)$, the potential slow roll parameters can be calculated as

$$\epsilon_V(\chi) = \frac{M_{\rm pl}^2}{2} \left(\frac{dU/d\chi}{U(\chi)} \right)^2 , \qquad \eta_V(\chi) = M_{\rm pl}^2 \left(\frac{d^2U/d\chi^2}{U(\chi)} \right) . \tag{4.13}$$

The field value corresponding to the end of inflation $\chi_{\rm end}$ is obtained by setting $\epsilon_V = 1$, while the horizon exit value $\chi_{\rm in}$ can be calculated assuming 60 e-foldings between the two periods.

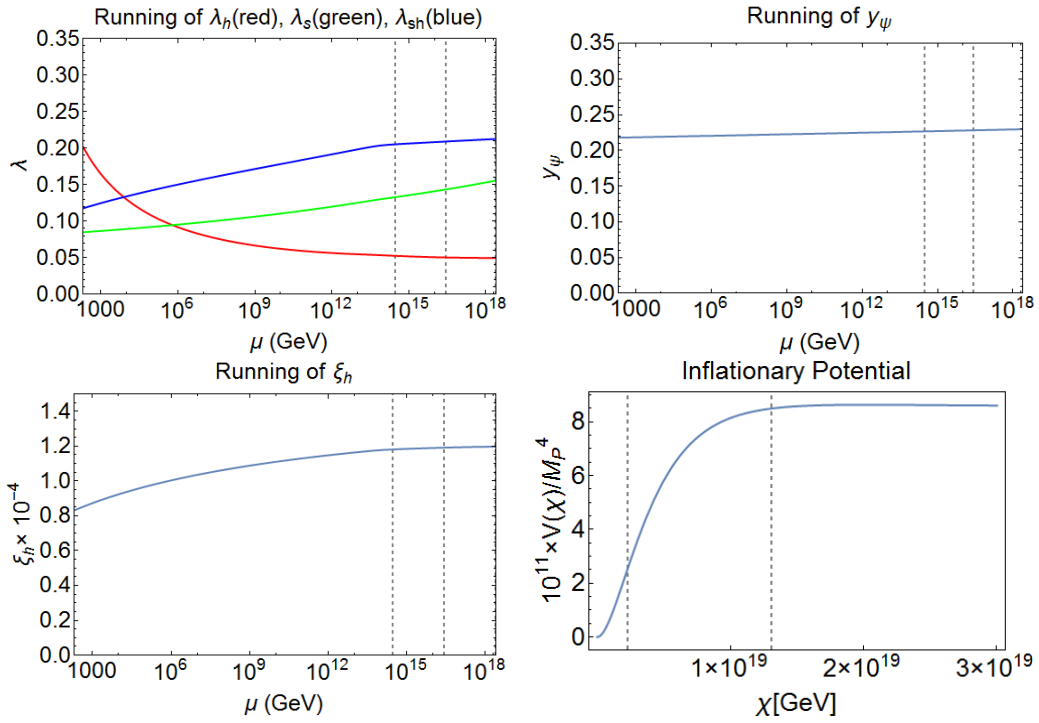

Figure 4.1: Running behavior and shape of potential for $h-$inflation for (approximate) parameter values $\{m_s, m_\psi, u\} = \{450, 235, 1080\}$ GeV and $\{\lambda_h, \lambda_s, \lambda_{sh}, \varphi\} = \{0.17, 0.08, 0.12, 0.17\}$. The plot on the top left shows the running of λ_h, λ_s and λ_{sh}. The plot on the top right shows the running of y_ψ. The bottom left plot shows the running of nonminimal coupling ξ_h, and the bottom right plot shows the inflationary potential. In the first three plots, the vertical dashed lines correspond to $M_{\rm pl}/\xi_h$ (left) $M_{\rm pl}/\sqrt{\xi_h}$ (right). In the fourth plot, they correspond to the scales of end of inflation (left) and horizon exit (right).

$$N_{\text{e-folds}} = \int_{\chi_{\text{end}}}^{\chi_{\text{in}}} d\chi \frac{1}{M_{\text{pl}}\sqrt{2\epsilon_V}} \,. \tag{4.14}$$

This allows us to calculate the inflationary observables n_s and r as

$$\begin{aligned} n_s &= 1 + 2\eta_V - 6\epsilon_V \,, \\ r &= 16\epsilon_V \,, \end{aligned} \tag{4.15}$$

as well as the amplitude of scalar fluctuations $\Delta^2_{\mathcal{R}}$ as

$$\Delta^2_{\mathcal{R}} = \frac{1}{24\pi^2 M^4_{\text{pl}}} \frac{U(\chi)}{\epsilon_V} = 2.2 \times 10^{-9} \,. \tag{4.16}$$

As mentioned earlier, the last constraint, coming from CMB observations [2], is used to determine ξ_h.

For inflation to occur, we require the Higgs potential to be stable, i.e, $\lambda_h(\mu) > 0$ for all scales μ up to the scale of inflation. For the standard model Higgs, this condition is not satisfied unless the top quark Yukawa coupling y_t is set to about three standard deviations below its measured central value. In our model, λ_h receives a positive threshold correction at the m_s scale and also a positive contribution to the beta function from λ_{sh}, therefore the constraint on y_t coming from requiring the stability of Higgs potential is removed. In fact, we impose a more restrictive constraint of requiring that the inflationary potential be monotonically increasing with h (or χ) for the entire range of field values relevant during and immediately after inflation. This is done to ensure that slow roll drives the Higgs field towards the electroweak vacuum and not away from it, and amounts to preventing λ_h/ξ_h^2 from decreasing too quickly at high scales.

4.3.2 $s-$Inflation

Much of the discussion in the previous section carries over to the $s-$inflation case, except that the roles of the h and s fields are interchanged. We input the same parameters (m_s, φ, λ_{sh}, y_ψ) at the electroweak scale as before.

The 1-loop corrected Einstein frame action for s-inflation (along the s-axis) is given by

$$S_{\rm inf} = \int d^4x\sqrt{\tilde{g}}\left[\frac{M_{\rm pl}^2}{2}R + \frac{1}{2}\left(\partial\chi\right)^2 - U(\chi)\right], \tag{4.17}$$

with potential

$$U(\chi) = \frac{\lambda_s\left(s(\chi)\right)^4}{4\Omega^4}, \tag{4.18}$$

where the new field χ is now

$$\frac{d\chi}{ds} = \sqrt{\frac{3M_{\rm pl}^2\left(d\Omega^2/ds\right)^2}{2\Omega^4} + \frac{1}{\Omega^2}} \approx \sqrt{\frac{1+\xi_s s^2/M_{\rm pl}^2 + 6\xi_s^2 s^2/M_{\rm pl}^2}{\left(1+\xi_s s^2/M_{\rm pl}^2\right)^2}}. \tag{4.19}$$

The running couplings and the inflationary potential for a typical data point for $s-$inflation are shown in Figs 4.2.

For stability of the inflationary potential, we now require λ_s to be positive at scales relevant to inflation, and for $U(\chi)$ monotonically increasing with χ. In this case, we do not try to avoid the instability of the potential in the Higgs direction since we do not expect this region of the potential landscape to be explored during or after inflation; the field rolls along the s-axis until the electroweak scale, where it runs off the axis and eventually settles in the electroweak vev which is a minimum along both field directions.

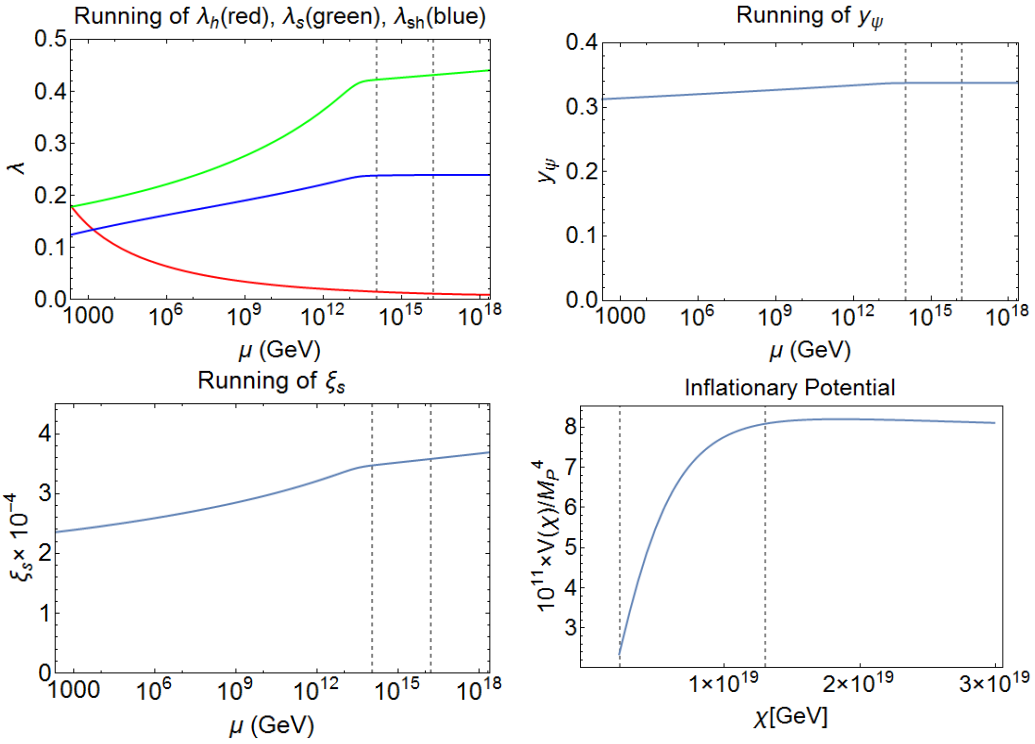

Figure 4.2: Running behavior and shape of potential for $s-$inflation for (approximate) parameter values $\{m_s, m_\psi, u\} = \{493, 257, 823\}$ GeV and $\{\lambda_h, \lambda_s, \lambda_{sh}, \varphi\} = \{0.15, 0.18, 0.12, 0.11\}$. The plot on the top left shows the running of λ_h, λ_s and λ_{sh}. The plot on the top right shows the running of y_ψ. The bottom left plot shows the running of nonminimal coupling ξ_s, and the bottom right plot shows the inflationary potential. In the first three plots, the vertical dashed lines correspond to $M_{\rm pl}/\xi_s$ (left) $M_{\rm pl}/\sqrt{\xi_s}$ (right). In the fourth plot, they correspond to the scales of end of inflation (left) and horizon exit (right).

4.3.3 Consistency constraints

In addition to requiring the stability of the inflaton potential, there are further constraints that are necessary to consider in order to ensure the consistency of the model.

Perturbativity of λ's: One observation to make is that unlike in the case of the standard model λ_h, which usually decreases at high scales (the beta function evaluates to negative values), in our model λ_h, λ_s and λ_{sh} often run to larger values. Therefore, it is necessary to ensure these couplings stay small enough to avoid nonperturbative effects. We impose $|\lambda_h| < 1$, $|\lambda_s| < \sqrt{4\pi}$ and $|\lambda_{sh}| < \sqrt{4\pi}$ at all scales. This constraint typically restricts the couplings to take small values, $0 < \lambda_s, \lambda_{sh} < 0.3$ at the electroweak scale.

Isocurvature Modes For both $h-$inflation and $s-$inflation, we assumed we have an effectively single field slow roll scenario. This is applicable only when the potential is both curved upwards and sufficiently steep in the transverse direction during inflation. For Higgs inflation (and similarly for $s-$inflation), we can write the transverse (isocurvature) mass as

$$m_{\rm iso}^2 \approx \frac{\lambda_{sh} h^2}{\Omega^2}\,. \tag{4.20}$$

where we have assumed that ξ_s is small, in order to suppress a negative contribution from the λ_h term.

For consistency, we require this quantity to be positive and much larger

than the typical Hubble parameter during inflation

$$H_{\rm inf}^2 = \frac{1}{3}\frac{U(\chi)}{M_{\rm pl}^2}\,. \tag{4.21}$$

We observe that $m_{\rm iso}$ typically evaluates to be of $\mathcal{O}(10^{16})\,\text{GeV}$ whereas $H_{\rm inf}$ typically comes to be of $\mathcal{O}(10^{13})\,\text{GeV}$. Therefore, this constraint is easily satisfied in our model for both $h-$ and $s-$inflation given that the less relevant non-minimal coupling is small enough.

4.4 Phenomenological Constraints

After the end of inflation, we expect the inflaton to execute oscillations about the minimum of its potential and eventually settle at its minimum after transferring most of the energy into excitations of the various standard model (and dark matter) fields. A detailed analysis of reheating in the case of standard Higgs inflation was done in [22]. In our model, for typical values of the various input parameters, we expect a similar process to happen for both h-inflation and s-inflation. Moreover, as long as the Yukawa coupling y_ψ and mixing angle φ are not unnaturally small, we can expect dark matter to enter into thermal equilibrium with the standard model particles, thus following the usual WIMP scenario. Since the value of the inflaton field is at this stage much smaller than $M_p/\sqrt{\xi}$, the nonminimal coupling to gravity is practically irrelevant for this discussion. Our model then reduces to a special case of the singlet scalar+fermion dark matter model discussed in [50, 79, 87, 98] with the terms having odd powers of s set to zero.

4.4.1 Dark Matter Relic Density

Assuming all the (cold) dark matter in the universe is accounted for by our fermionic dark matter candidate ψ, we require its relic density to agree with the Planck measurements $\Omega_c h^2 = 0.1198 \pm 0.0015$ [1].

Using the dark matter annihilation cross section derived in Appendix D, the thermally averaged cross section as a function of $x = m_\psi/T$ can be written as [61]

$$\langle \sigma\, v_{rel} \rangle (x) = \frac{x}{16 m_\psi^5 K_2^2(x)} \int_{4m_\psi^2}^{\infty} ds\, s^{3/2} \sigma v \sqrt{1 - \frac{4m_\psi^2}{s}}\, K_1\left(\frac{\sqrt{s}}{m_\psi} x\right), \quad (4.22)$$

where K_1 and K_2 are modified Bessel functions. The freezout value $x = x_f$ can be calculated iteratively [50, 79, 98] using the relation

$$x_f = \log\left(\frac{3 M_{\rm pl}}{\pi^2} \sqrt{\frac{5 m_\psi^2}{\pi g_* x_f}}\, \langle \sigma\, v_{rel}(x_f) \rangle \right). \quad (4.23)$$

The relic density is then calculated using

$$\Omega_c h^2 \simeq \frac{\left(2.13 \times 10^8\, \mathrm{GeV}^{-1}\right)}{\sqrt{g_*} M_{\rm pl}\, \mathcal{J}(x_f)}, \quad (4.24)$$

where all mass dimensions are expressed in GeV and the integral $\mathcal{J}$ is given by

$$\mathcal{J}(x_f) = \int_{x_f}^{\infty} dx \frac{\langle \sigma\, v_{rel}(x) \rangle}{x^2}. \quad (4.25)$$

We performed the last integral by evaluating the function $\langle \sigma\, v_{rel}(x) \rangle$ by using an interpolation. This integral is often approximated by assuming $\langle \sigma\, v_{rel}(x) \rangle$ to be a constant or a simple function of x; however, it was shown

in [66] that such approximations break down near the resonance region of the cross section. Since our results (Figure 4.5) indicate that the surviving parameter space of our model largely falls near the resonance region, these approximations do not serve our purposes.

4.4.2 Direct Detection Constraint

Calculation of direct detection cross section for our model proceeds in the same way as in [50]. We define the effective coupling of dark matter to protons and neutrons as

$$\begin{aligned} f_p &= m_p \bar{\alpha} \left(f_{Tu}^p + f_{Td}^p + f_{Ts}^p + \frac{2}{9} f_{Tg}^p \right) , \\ f_n &= m_n \bar{\alpha} \left(f_{Tu}^n + f_{Td}^n + f_{Ts}^n + \frac{2}{9} f_{Tg}^n \right) , \end{aligned} \tag{4.26}$$

where m_p and m_n are the masses of proton and neutron respectively, and $\bar{\alpha}$ is defined as

$$\bar{\alpha} = \frac{y_\psi \sin 2\varphi}{2v} \left(\frac{1}{m_h^2} - \frac{1}{m_s^2} \right) . \tag{4.27}$$

For the hadronic matrix elements, we use the central values from [49],

$$\begin{aligned} &f_{Tu}^p = 0.020 , \quad f_{Td}^p = 0.026 , \quad f_{Ts}^p = 0.118 , \quad f_{Tg}^p = 0.84 , \\ &f_{Tu}^n = 0.014 , \quad f_{Td}^n = 0.036 , \quad f_{Ts}^n = 0.118 , \quad f_{Tg}^n = 0.83 . \end{aligned} \tag{4.28}$$

The spin-independent cross section per nucleon can be obtained as

$$\sigma_{SI} = \frac{m_\psi^2 + m_N^2}{m_\psi^2 + m_p^2} \frac{m_\psi^2 m_p^2}{(m_\psi + m_N)^2} \frac{4}{\pi A^2} \left(Z f_p + (A - Z) f_n \right)^2 , \tag{4.29}$$

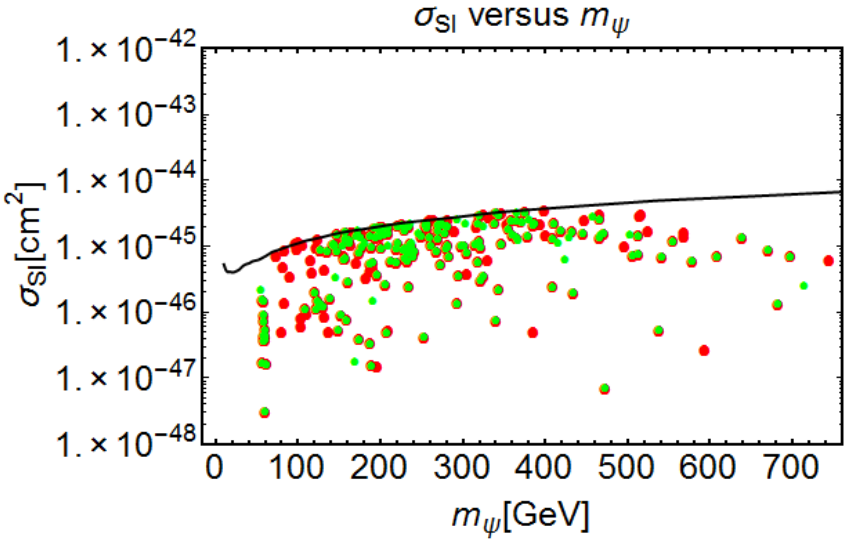

Figure 4.3: Spin independent direct detection cross section σ_{SI} plotted as a function of dark matter mass. The black line corresponds the the LUX bound. The green and red points correspond to h-inflation and s-inflation respectively.

where Z, A and m_N are the atomic number, atomic mass (number) and nuclear mass respectively of the target nucleus in the direct detection experiment. We then restrict our parameter space using the (Xenon-based) LUX bounds [7] which are the most restrictive bounds currently available. The cross section for our surviving data points has been shown in Figure 4.3.

4.4.3 Collider Constraints

We impose two constraints coming from collider phenomenology in our study. The first is the Electroweak Precision Test (EWPT) constraint [18], which provides an upper bound for the value of mixing angle φ as a function of the scalar mass m_s for the entire range of scalar mass we consider. While the

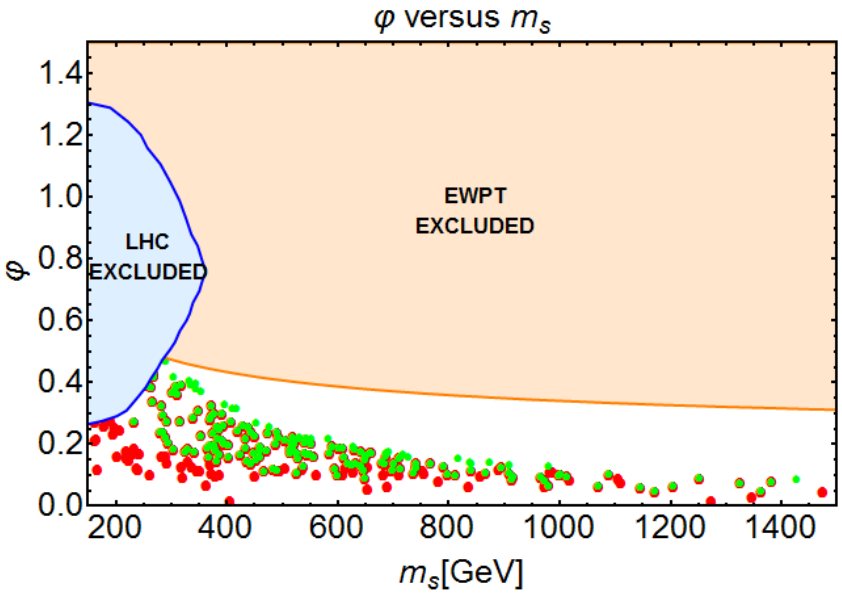

Figure 4.4: Comparison of mixing angle φ as a function of mass of the scalar field at its low energy vacuum, m_s. The orange line corresponds to the EWPT upper bound on φ and the blue line corresponds to LHC physics lower bound on m_s. The orange and blue shaded regions are excluded by these bounds respectively. The green points correspond to $h-$inflation (λ_h) and the red points correspond to $s-$inflation (λ_s).

constraint allows for both positive and negative values of φ, we are required to restrict to just positive values so as to ensure that $\lambda_{sh} > 0$ (which is necessary to avoid isocurvature fluctuations).

The second constraint we consider comes from LHC physics. The allowed mass region for a high mass scalar S that has the decay channel $S \to WW$ and $S \to ZZ$ was analyzed in [34], and this analysis was later recast for the scalar mass into a constraint in the $m_S - \varphi$ plane in [108] yielding this exclusion limit at 95% CL. Both these constraints are shown in Figure

4.4.

4.5 Numerical Results

In our analysis, we begin by allowing the scalar mass m_s to vary between 150-1500 GeV and the dark matter mass m_ψ to vary between 50-1500 GeV. The mixing angle φ is bounded by the LHC and the EWPT constraints and is taken to be positive, while the quartic coupling λ_{sh} is allowed to vary between 0 and 1. The remaining parameters - u, y_ψ, λ_h, λ_s - are constrained by these requirements. Further, we impose the (Planck) relic density and the (LUX) direct detection constraints, as well as the perturbativity constraint, i.e, $\lambda_s, \lambda_{sh} < \sqrt{4\pi}$ and $\lambda_h < 1$ at all scales, on all the points. All these constraints are imposed on all parameter points uniformly.

Apart from these, for each type of inflation ($h-$ or $s-$), we also impose the stability constraint of requiring that the appropriate self coupling $\lambda > 0$ all the way up to inflationary scale. We also constrain the potential along the inflation axis to monotonically increase with scale in the inflationary region, so as to ensure that the slow roll happens towards, and not away from the low energy vacuum.

In all our plots including both types of inflation, the green points correspond to $h-$inflation and the red points correspond to $s-$inflation. There are many points that survive both sets of constraints, indicated by green points coincident with red; these points have a stable potential along both axes and allow successful $h-$inflation as well as $s-$inflation.

In the first plot in Figure 4.5, we show the dark matter mass as a function of the the scalar mass for points that survive the above constraints. We note that the dark matter mass tends to take values near two straight lines. These lines correspond to resonance regions, where the dark matter mass is either half of the Higgs mass or half the scalar mass. Previous studies of similar models [50, 87] indicate that the relic density and direct detection constraints can be satisfied by points that are on or near the resonance region as well as points that are off the resonance region. In our model, owing to the absence of a Dirac mass for dark matter, fixing m_ψ also fixes the value of y_ψ. Since we also require the perturbativity of the couplings and the stability of the potential, the allowed range of values for y_ψ is limited (generally < 0.7) and therefore the constraints end up allowing only points near the resonance region which have a smaller value of y_ψ and are consistent with absence of Dirac mass.

In Figure 4.6, we have shown the starting (electroweak scale) values of the self couplings λ_h and λ_s. The points that allow successful h-inflation tend to have larger values of λ_h. This is not surprising given the requirement that the potential be stable along the $h-$axis for $h-$inflation. This is also consistent with the the second plot (top right) in Figure 4.6 comparing the starting (electroweak) value of λ on the inflation axis with the value of the same λ at inflationary scale. This plot indicates that the inflationary value of λ (λ_h or λ_s) is strongly correlated to the electroweak value of the same λ. The plot also shows that for $s-$inflation, λ_s generally runs to larger values irrespective of

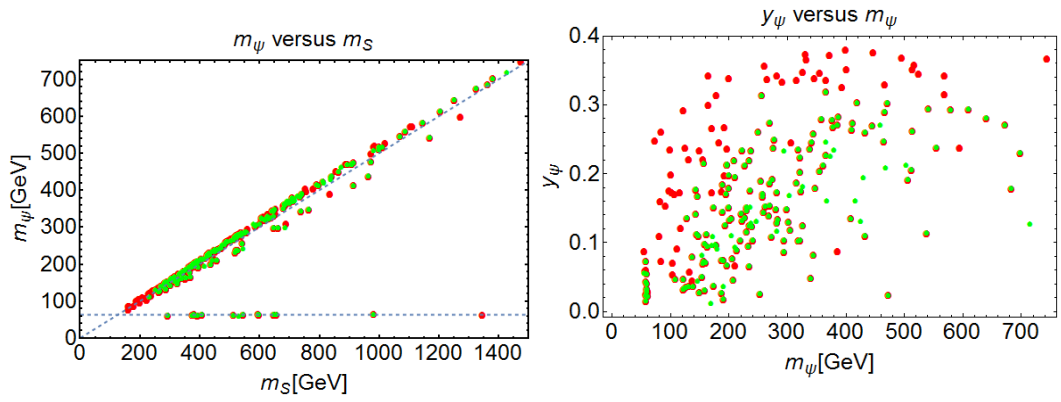

Figure 4.5: On the left side, dark matter mass m_ψ plotted against the scalar mass m_s. The dashed lines correspond to $m_\psi = (1/2)m_s$ and $m_\psi = (1/2)m_h$ respectively. On the right side, the dark matter Yukawa coupling y_ψ is plotted against dark matter mass m_ψ. The green points correspond to $h-$inflation and the red points correspond to $s-$inflation. Note that many green points coincide with red points, indicating a potential that can support both $h-$inflation and $s-$inflation.

its starting value, whereas for $h-$ inflation, λ_h can run upwards or downwards depending on whether the starting value is large or small. Therefore, if λ_h does not start out with a sufficiently large value, it could run to negative values (which is indeed the problem with the standard model Higgs potential).

The third plot (bottom left) in Figure 4.6 showing mixing angle φ as a function of the quartic coupling λ_{sh} indicates that the mixing angle tends to be larger for the Higgs inflation points. This is, again, expected because the standard model Higgs potential is unstable and the mixing angle should be large enough to allow λ_h to stay positive. The s-potential does not necessarily have such an instability, and therefore it is less dependent on the λ_{sh}^2 term in its beta-function for stability.

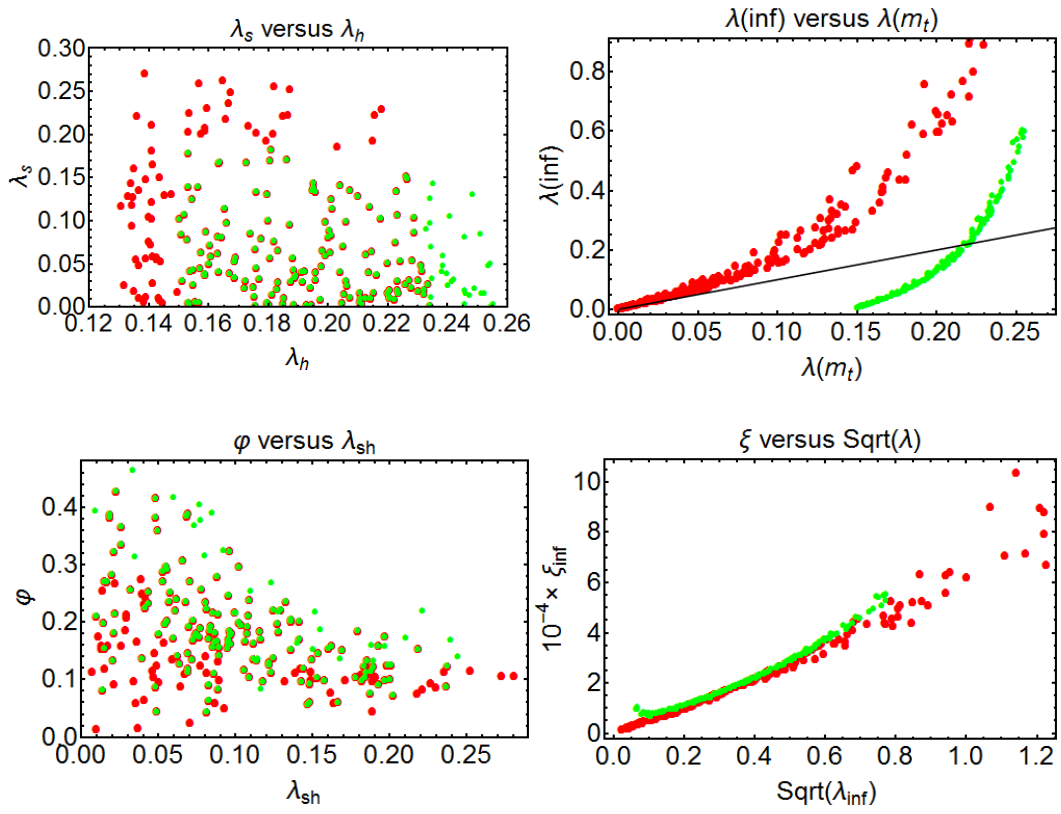

Figure 4.6: The figure on the top left compares λ_h and λ_s at the electroweak scale. The figure on top right shows the λ at the inflationary scale as compared to λ at the electroweak scale, with λ being either λ_h or λ_s for $h-$ or $s-$inflation respectively (the black line corresponds to $y = x$). The figure on the bottom left shows mixing angle φ versus λ_{sh} at the electroweak scale. The figure on the bottom right shows $\sqrt{\lambda}$ as a function of nonminimal coupling ξ, both evaluated at the scale of inflation. In all the plots, the green points correspond to $h-$inflation and the red points correspond to $s-$inflation.

The fourth plot in Figure 4.6 compares ξ to $\sqrt{\lambda}$ along the inflationary axis and shows an approximate linear behavior. Given that the inflationary potential at large scales is proportional to λ/ξ^2 and the slow roll parameter ϵ_V at that scale is approximately the same order of magnitude for all our data points, this correlation is consistent with imposing the constraint from $\Delta^2_{\mathcal{R}}$ in Eq. (4.15).

Figure 4.7 showing $n_s - r$ predictions for $h-$ and $s-$ inflation is the main result/prediction from this model. From the plot we can see that inflationary predictions for h- and $s-$inflation are not markedly different. This is expected, because at the inflationary scale, both types of inflation involve a scalar field with a quartic potential and quadratic nonminimal coupling to gravity; the running behavior does not significantly affect results. It is also clear that our model generically predicts low tensor to scalar ratio and therefore most of our data points are well within the region selected by Planck.

4.6 Conclusions

In this chapter, we studied a model of inflation that involves a gauge singlet scalar and fermionic dark matter. The mixing between the Higgs and the scalar singlet provides a portal to dark matter. Either the singlet scalar or the Higgs plays the role of the inflaton field, with the non-minimal coupling to gravity providing the correct shape of the potential for realizing successful inflation.

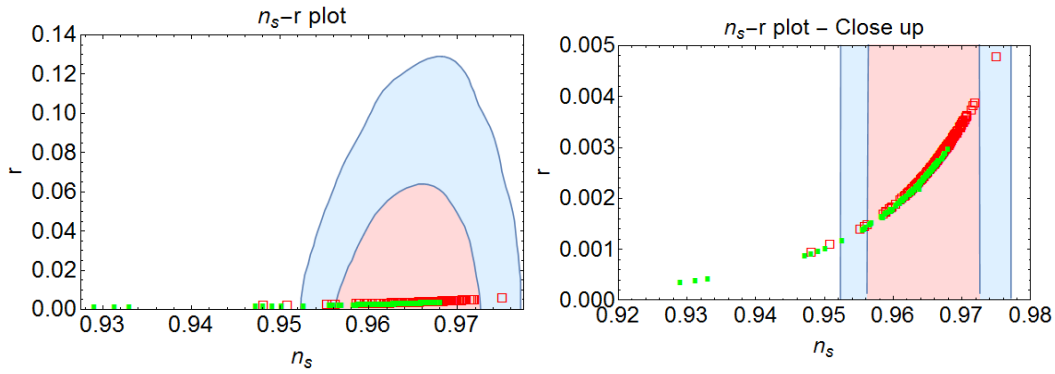

Figure 4.7: $n_s - r$ values for $h-$inflation and $s-$inflation. The plot on the left shows the complete range of Planck 68% (red) and 95% (blue) confidence limits, while the right plot zooms into the location of our data points. The filled green points (squares) correspond to $h-$inflation and the empty red points correspond to $s-$inflation.

1. We considered the simplest case of the inflaton rolling along the Higgs-axis ($h-$ inflation) or the scalar axis ($s-$inflation). Both types of inflation generically produce $n_s - r$ values consistent with current Planck bounds.

2. Both types of inflation generically yield small values of tensor-to-scalar ratio comparable to tree level Higgs inflation models, and a wide range of n_s values including those outside of the Planck allowed regions.

3. The stability of the Higgs potential can be easily restored through the coupling with the singlet scalar.

4. The dark matter and perturbativity/stability constraints ensure that only points near the resonance regions, $m_\psi = \frac{1}{2}m_s$ or $m_\psi = \frac{1}{2}m_h$, successfully satisfy all the constraints. This is a significant restriction on

the parameter space.

5. The new scalar mass can be as small as 200 GeV or as large as $\mathcal{O}$(TeV). For smaller masses, the mixing angle with the Higgs is less constrained while for larger masses the angle must be small enough due to decoupling behavior.

6. Due to different running behavior on λ_h and λ_s, the upper bound on mixing angle coming from the perturbativity requirement is more constraining (lower) for $s-$inflation, while the lower bound coming from the stability requirement is more constraining (higher) for $h-$inflation, as seen from Fig. 4.4.

It is interesting to see that the favored parameter region could be further explored in near future. The constraint on the dark matter direct detection cross section is set to become more restrictive in the coming years. Similarly, the new run of LHC is expected to constrain the allowed range of mixing angle φ for larger values of m_s. Based on Figs. 4.3 and 4.4, it is clear that this would certainly restrict our parameter space further. Moreover, the ongoing and upcoming CMB B-mode searches are expected to detect or further constrain the tensor-to-scalar ratio in the coming years, which could improve the distinguishing power between different inflationary models. The inflationary predictions of our model could potentially be verified with this higher level of sensitivity.

Chapter 5

Conclusions

The paradigm of inflation continues to hold great promise for active research by offering many different avenues to probe its nature. There are many ongoing and future experiments that probe early universe, most notably polarization experiments[1] and LSS experiments[2] which can be expected to constrain and rule out many inflationary models in coming decade. Moreover, models that connect inflation to standard model and dark matter phenomenology are subject to even better observational validation through the various dark matter probes. In this dissertation, we discussed a few of these avenues for constraining models of the early universe.

In the second chapter, we showed how CMB power spectrum observations already put stringent bounds on Bogoliubov excitations in the inflationary spectrum. This indicates that such excitations in themselves cannot be large enough to generate an observable effect on the measured local (squeezed limit) f_{NL}. These strict bounds also tell us that drastic pre-inflationary equation of state transitions such as sudden transitions from Kinetic energy dominated phase to inflation cannot consistently account for the observed CMB

[1] A fairly comprehensive list of polarization experiments has been given in [76].
[2] For a fairly recent review of LSS experiments and their prospects, see [9].

spectrum. Therefore, if such transitions occurred they must have occurred sufficiently long before horizon-exit of inflationary modes or sufficiently slowly so that any modes significantly affected by the transition are outside the horizon.

In the third chapter, we discussed our study of tunneling out of a metastable vacuum in multi-dimensional field theory and the dependence of the bounce action on the number of fields. By using scaling relations and exact solutions, we were able to get insights into estimating the bounce action given a bounce trajectory. We also showed that determining the bounce trajectory remains a difficult problem, given that tunneling could take place along the direction of larger barrier making the common intuitive approach misleading.

In the fourth chapter, we discussed a model that involved the standard Higgs inflation scenario modified by adding new singlet scalar and fermionic dark matter. We showed that the parameter space of such models can be considerably constrained by dark matter constraints and other phenomenological constraints in concert with the requirements for producing successful inflation; in particular we noted that the mass of the dark matter particle had to lie near the resonance region (half the Higgs or scalar masses) in order for the all the constraints to be satisfied.

In summary, this dissertation discussed a few of the many different ways of probing the nature of the inflationary universe. As mentioned previously, there are many different experiments collecting precision data that is continually improving our understanding of this phase of the universe. Depending on whether we have a detection or just tighter upper bounds on tensor modes

and other observables, the direction in which this field proceeds can change dramatically over the next few years. Therefore, at the very least, it is reasonable to state that this area of research still has a lot of scope for asking meaningful and answerable questions.

Appendices

Appendix A

Squeezed Limit Bispectrum For Excited States[1]

To compute the bispectrum up to tree level, we follow the approach in [91]. The operator $\hat{\mathcal{R}}(\mathbf{k},t)$ is defined the same way as in the standard case (given in (1.9)), with the mode function of the form (2.1), corresponding to an excited state rather than the Bunch-Davies state. This results in the following general expression (which has also been derived earlier, for example see [57, 58, 73]) for the bispectrum

$$\begin{aligned}
\langle \mathcal{R}_{\mathbf{k}_1}\mathcal{R}_{\mathbf{k}_2}\mathcal{R}_{\mathbf{k}_3}\rangle &= (2\pi)^3\delta\left(\mathbf{k}_1+\mathbf{k}_2+\mathbf{k}_3\right)\left(\prod_a \frac{1}{2k_a^3}\right) A_{k_1k_2k_3} \\
A_{k_1k_2k_3} &= \frac{2H^6}{\dot{\phi}^2}\left(\sum_{i\neq j} k_i^2k_j^2\right) Re\left[M_{k_1k_2k_3}\right] + \frac{H^8}{\dot{\phi}^4}\left(\prod_i |\alpha_{k_i}+\beta_{k_i}|^2\right) N_{k_1k_2k_3} \\
M_{k_1k_2k_3} &= \prod_m \left(\alpha^*_{k_m}+\beta^*_{k_m}\right)\left[\frac{\alpha_{k_1}\alpha_{k_2}\alpha_{k_3}-\beta_{k_1}\beta_{k_2}\beta_{k_3}}{k_1+k_2+k_3}\right. \\
&\qquad \left. + \left\{\frac{\alpha_{k_1}\alpha_{k_2}\beta_{k_3}-\beta_{k_1}\beta_{k_2}\alpha_{k_3}}{k_1+k_2-k_3}+\text{cyclic}\right\}\right]
\end{aligned}$$

[1]Portions of this appendix have been previously published in [12]

$$N_{k_1k_2k_3} = \frac{2\ddot{\phi}}{H\dot{\phi}}\sum_i \frac{k_i^3}{|\alpha_{k_i}+\beta_{k_i}|^2} + \frac{1}{2}\frac{\dot{\phi}^2}{H^2}\left[\sum_i \frac{k_i^3}{|\alpha_{k_i}+\beta_{k_i}|^2} + \sum_{i\neq j}\frac{k_i k_j^2}{|\alpha_{k_i}+\beta_{k_i}|^2}\right], \tag{A.1}$$

where $\alpha_{k_i} = \alpha(k_i)$ and $\beta_{k_i} = \beta(k_i)$ are the Bogoliubov parameters.

The relative magnitude of the bispectrum in comparison to the power spectrum can be written in terms of f_{NL} [21] as

$$\mathcal{B}_{\mathcal{R}}(k_1,k_2,k_3) = \frac{6}{5}f_{NL}^{local} \times \left[P_{\mathcal{R}}(k_1)P_{\mathcal{R}}(k_2) + P_{\mathcal{R}}(k_2)P_{\mathcal{R}}(k_3) + P_{\mathcal{R}}(k_3)P_{\mathcal{R}}(k_1)\right]. \tag{A.2}$$

There is no convenient k-independent parameter f_{NL} that can be defined for a general set of momenta. In the squeezed limit for the shape of the triangle, where $\{k_1,k_2,k_3\} \to \{k_s,k_s,k_l\}$ (with the subscripts l and s standing for momenta with long or short wavelengths) where $k_s \gg k_l$, we use the relation

$$\lim_{k_s\gg k_l} \mathcal{B}_{\mathcal{R}}(k_s,k_s,k_l) = \frac{12}{5}f_{NL}^{local}P_{\mathcal{R}}(k_s)P_{\mathcal{R}}(k_l) \tag{A.3}$$

to obtain the squeezed-limit f_{NL}. This can be used to obtain an expression for f_{NL} in terms of α and β. However, to get from here to an exact f_{NL} expression that can be compared to measurements, we need to integrate over momenta, similar to what is discussed in [57].

Appendix B

Beta Functions[1]

The following are the one-loop beta functions used for the various parameters in the Lagrangian for our Higgs portal model in Chapter 4. Here, we use the electroweak scale values of the various couplings consistent with [30].

$$
\begin{aligned}
\beta_{g_s} &= \frac{g_s^3}{(4\pi)^2}(-7) + \frac{g_s^3}{(4\pi)^4}\left(\frac{11}{6}g'^2 + \frac{9}{2}g^2 - 26g_s^2 - 2x_\phi y_t^2\right), \\
\beta_g &= \frac{g^3}{(4\pi)^2}\left(-\frac{39 - x_\phi}{12}\right) + \frac{g^3}{(4\pi)^4}\left(\frac{3}{2}g'^2 + \frac{35}{6}g^2 + 12g_s^2 - \frac{3}{2}x_\phi y_t^2\right), \\
\beta_{g'} &= \frac{g'^3}{(4\pi)^2}\left(\frac{81 + x_\phi}{12}\right) + \frac{g'^3}{(4\pi)^4}\left(\frac{199}{18}g'^2 + \frac{9}{2}g^2 + \frac{44}{3}g_s^2 - \frac{17}{6}x_\phi y_t^2\right), \\
\beta_{\lambda_h} &= \frac{1}{(4\pi)^2}\Bigg(6(1 + 3x_\phi^2)\lambda_h^2 - 6y_t^4 + \frac{3}{8}(2g^4 + (g^2 + g'^2)^2) \\
&\qquad\qquad + \lambda_h(-9g^2 - 3g'^2 + 12y_t^2) + \frac{1}{2}\lambda_{sh}^2 x_s^2\Bigg), \\
\beta_{\lambda_{sh}} &= \frac{\lambda_{sh}}{(4\pi)^2}\left(12x_\phi^2\lambda_h + 4x_\phi x_s\lambda_{sh} + 6x_s^2\lambda_s + 6y_t^2 + 2y_\psi^2 - \frac{9}{2}g^2 - \frac{3}{2}g'^2\right), \\
\beta_{\lambda_s} &= \frac{1}{(4\pi)^2}(18x_s^2\lambda_s^2 + 4\lambda_s y_\psi^2 + 2x_\phi^2\lambda_{sh}^2 - 2y_\psi^4), \\
\beta_{y_\psi} &= \frac{y_\psi^3}{(4\pi)^2}\left(\frac{9x_s}{2}\right), \\
\beta_{y_t} &= \frac{y_t}{(4\pi)^2}\left[-\frac{9}{4}g^2 - \frac{17}{12}g'^2 - 8g_s^2 + \frac{23 + 4s}{6}y_t^2\right], \\
\beta_{\xi_h} &= \frac{1}{(4\pi)^2}\left(\xi_h + \frac{1}{6}\right)\left[-\frac{3}{2}g'^2 - \frac{9}{2}g^2 + 6y_t^2 + (6 + 6x_\phi)\lambda_h + \lambda_{sh}\right],
\end{aligned}
$$

[1]Portions of this appendix have been previously published in [16]

$$\beta_{\xi_s} = \frac{1}{(4\pi)^2}\left(\xi_s + \frac{1}{6}\right) \times \left[6x_s\lambda_s + (x_\phi + 3)\lambda_{sh}\right] . \tag{B.1}$$

Here, g, g' and y_t are the standard model $SU(2)$, $U(1)$ and top-quark Yukawa couplings, while the $x's$ are defined as

$$\begin{aligned} x_\phi &= \frac{1 + \xi_h h^2/M_{\rm pl}^2}{1 + \xi_h h^2/M_{\rm pl}^2 + 6\xi_h^2 h^2/M_{\rm pl}^2} , \\ x_s &= \frac{1 + \xi_s s^2/M_{\rm pl}^2}{1 + \xi_s s^2/M_{\rm pl}^2 + 6\xi_s^2 s^2/M_{\rm pl}^2} . \end{aligned} \tag{B.2}$$

Appendix C

Conformal Transformation[1]

Here is a brief description of conformal transformations that we use to deal with theories involving non-minimal coupling to gravity, such as the model discussed in Chapter 4.

On performing an arbitrary conformal transformation $g \to \tilde{g} = \Omega^2 g$, the Ricci scalar transforms as

$$R[g] = \Omega^2 R[\tilde{g}] - 6\Omega\tilde{\Box}\Omega, \tag{C.1}$$

where $R[g]$ is the Ricci scalar as a function of the metric g, and $\tilde{\Box}$ is the d'Alembertian for metric $\tilde{g}$. The inhomogeneous part serves to modify the kinetic term of the quantum fields.

Starting with the action in Jordan frame

$$S_J = \int d^4x \, \sqrt{-g} \left[-\frac{M_P^2}{2} R[g] f(\phi) + \frac{1}{2} g^{\mu\nu} \partial_\mu \phi \partial_\nu \phi \right], \tag{C.2}$$

we can get rid of the non-minimal coupling by peforming a conformal transformation with

$$\Omega^2 = f(\phi), \tag{C.3}$$

[1]Portions of this appendix have been previously published in [16]

with the following modification of the scalar kinetic term

$$\mathcal{L}_{\rm kin} = \frac{1}{2}\left[\frac{3M_P^2(d\Omega^2/d\phi)^2}{2\Omega^4} + \frac{1}{\Omega^2}\right](\partial\phi)^2\,. \tag{C.4}$$

This means that the field content in this theory ϕ is no longer canonically normalized. In order to compute quantum corrections, we define a rescaled canonically normalized field χ such that

$$\frac{d\chi}{d\phi} = \sqrt{\frac{3M_P^2(d\Omega^2/d\phi)^2}{2\Omega^4} + \frac{1}{\Omega^2}}, \tag{C.5}$$

which ensures that χ has a standard kinetic term.

In the case of multiple scalar fields, the kinetic term can be written in general as

$$\mathcal{L}_{\rm kin} = \frac{1}{2}\gamma^{ij}\partial_\mu\phi_i\partial^\mu\phi_j, \tag{C.6}$$

where

$$\gamma^{ij} = \frac{3M_P^2(d\Omega^2/d\phi_i)(d\Omega^2/d\phi_j)}{2\Omega^4} + \frac{1}{\Omega^2} \tag{C.7}$$

is the field space metric. Since this field-space metric can in general be intrinsically curved, the fields cannot be canonically normalized globally. However, if the field values in the theory are constrained to stay on (or close to) one of the field-axes, as we do in our Higgs portal model, the curved nature of the field space can be ignored.

Appendix D

Dark Matter Annihilation Cross Section[1]

In this section we calculate the annihilation cross section for dark matter in the model discussed in Chapter 4. For s-channel annihilation mediated by $\mathcal{H} = (h, S)$, the cross section has the form

$$\langle \sigma v_{\rm rel} \rangle(s) = \frac{\eta}{16\pi s} \times \beta_\psi \sum_f \left(\left| \sum_{r \in \mathcal{H}} \frac{y_r g_{f,r}}{s - m_r^2 + i m_r \Gamma_r} \right|^2 A_f \gamma_f \right) , \qquad \text{(D.1)}$$

where $\beta_i = (s - 4m_i^2)$ comes from the spin average of the initial dark matter state, and f runs over all the final states. The coupling $g_{f,r}$ is any coupling between final state f and the scalar $r \in \mathcal{H}$, and A_f is the spin structure of the final state f. η is $1/2$ for identical particles like ZZ, SS or hh and 1 otherwise; $\gamma_f = \sqrt{1 - \frac{4m_f^2}{s}}$ and $\gamma_{ij} = \sqrt{1 - \frac{2(m_i^2 + m_j^2)}{s} + \frac{(m_i^2 - m_j^2)^2}{s^2}}$ come from the phase space integration. For the cases we are interested in, we have $f = (q\bar{q},\, W^+W^-,\, ZZ,\, \mathcal{H}\mathcal{H})$:

$$\begin{aligned} A_{\mathcal{H}} &= 1 \,, \\ A_q &= N_c \times 2\beta_q \,, \\ A_{W,Z} &= \left(2 + \frac{(s - 2m_{W,Z}^2)^2}{4m_{W,Z}^4} \right) , \end{aligned} \qquad \text{(D.2)}$$

[1] Portions of this appendix have been previously published in [16]

where $N_c = 3$ for quark and $N_c = 1$ for lepton. The couplings $g_{f,r}$ are

$$
\begin{aligned}
y_r &= \frac{m_\psi}{v} \times \left\{ \begin{array}{ll} s_\varphi, & r = h\,, \\ c_\varphi, & r = s\,, \end{array} \right. \\
g_{q,r} &= \frac{m_q}{v} \times \left\{ \begin{array}{ll} c_\varphi, & r = h\,, \\ -s_\varphi, & r = s\,, \end{array} \right. \\
g_{W/Z,r} &= \frac{2m_{W/Z}^2}{v} \times \left\{ \begin{array}{ll} c_\varphi, & r = h\,, \\ -s_\varphi, & r = s\,, \end{array} \right. \\
\lambda_{hhh} &= -6\lambda_h v c_\varphi^3 - 3\lambda_{sh}(v c_\varphi s_\varphi^2 + u c_\varphi^2 s_\varphi) - 6\lambda_s u s_\varphi^3\,, \\
\lambda_{shh} &= 6\lambda_h v c_\varphi^2 s_\varphi - \lambda_{sh}(v(-1+3c_\varphi^2)s_\varphi + u c_\varphi(1-3s_\varphi^2)) - 6\lambda_s u c_\varphi s_\varphi^2\,, \\
\lambda_{ssh} &= -6\lambda_h v c_\varphi s_\varphi^2 - \lambda_{sh}(v c_\varphi(1-3s_\varphi^2) + u(1-3c_\varphi^2)s_\varphi) - 6\lambda_s u c_\varphi^2 s_\varphi\,, \\
\lambda_{sss} &= 6\lambda_h v s_\varphi^3 - 3\lambda_{sh}(-v c_\varphi^2 s_\varphi + u c_\varphi s_\varphi^2) - 6\lambda_s u c_\varphi^3\,,
\end{aligned}
\tag{D.3}
$$

where $c_\varphi \equiv \cos\varphi$ and $s_\varphi \equiv \sin\varphi$. When the final states are the scalars, we also have t, u channels and interference contributions:

$$
\begin{aligned}
\langle \sigma v_{\rm rel} \rangle_{ij}^{(t,u)} &= \frac{\eta}{16\pi s}\gamma_{ij} \times 2y_i^2 y_j^2 \Bigg[-2 + \frac{(4m_\psi^2 - m_i^2)(4m_\psi^2 - m_j^2)}{D^2 - A^2} \\
&\quad - \left\{ \frac{16m_\psi^4 - 4m_\psi^2 s - m_i^2 m_j^2}{2AD} + \frac{s + 8m_\psi^2 - m_i^2 - m_j^2}{2D} \right\} \log\left| \frac{A+D}{A-D} \right| \Bigg]\,, \\
\langle \sigma v_{\rm rel} \rangle_{ij}^{(int)} &= \frac{\eta}{16\pi s}\gamma_{ij} \times 4y_i y_j m_\psi \\
&\quad \times \left[-2 + \left\{ \frac{A}{D} + \frac{s - 4m_\psi^2}{D} \right\} \log\left| \frac{A+D}{A-D} \right| \right] \sum_{k \in \mathcal{H}} \frac{y_k \lambda_{ijk}(s - m_k^2)}{(s-m_k^2)^2 + m_k^2 \Gamma_k^2}\,,
\end{aligned}
$$

where A and D are defined as

$$
\begin{aligned}
A &= \frac{1}{2}(m_i^2 + m_j^2 - s)\,, \\
D &= \frac{1}{2}\sqrt{[s - (m_i + m_j)^2][s - (m_i - m_j)^2](s - 4m_\psi^2)/s}\,.
\end{aligned}
\tag{D.4}
$$

Bibliography

[1] P. A. R. Ade et al. Planck 2015 results. XIII. Cosmological parameters. 2015.

[2] P. A. R. Ade et al. Planck 2015 results. XX. Constraints on inflation. 2015.

[3] Nishant Agarwal, R. Holman, Andrew J. Tolley, and Jennifer Lin. Effective field theory and non-Gaussianity from general inflationary states. *JHEP*, 05:085, 2013.

[4] Ivan Agullo and Leonard Parker. Non-gaussianities and the Stimulated creation of quanta in the inflationary universe. *Phys. Rev.*, D83:063526, 2011.

[5] Ivan Agullo and Leonard Parker. Stimulated creation of quanta during inflation and the observable universe. *Gen. Rel. Grav.*, 43:2541–2545, 2011. [Int. J. Mod. Phys.D20,2861(2011)].

[6] Pontus Ahlqvist, Brian R. Greene, David Kagan, Eugene A. Lim, Saswat Sarangi, and I-Sheng Yang. Conifolds and Tunneling in the String Landscape. *JHEP*, 03:119, 2011.

[7] D. S. Akerib et al. Improved WIMP scattering limits from the LUX experiment. 2015.

[8] Kyle Allison. Higgs xi-inflation for the 125-126 GeV Higgs: a two-loop analysis. *JHEP*, 02:040, 2014.

[9] Marcelo Alvarez et al. Testing Inflation with Large Scale Structure: Connecting Hopes with Reality. 2014.

[10] Masato Arai, Shinsuke Kawai, and Nobuchika Okada. Higgs inflation in minimal supersymmetric SU(5) GUT. *Phys. Rev.*, D84:123515, 2011.

[11] Aditya Aravind, Brandon S. DiNunno, Dustin Lorshbough, and Sonia Paban. Analyzing multifield tunneling with exact bounce solutions. *Phys. Rev.*, D91(2):025026, 2015.

[12] Aditya Aravind, Dustin Lorshbough, and Sonia Paban. Non-Gaussianity from Excited Initial Inflationary States. *JHEP*, 07:076, 2013.

[13] Aditya Aravind, Dustin Lorshbough, and Sonia Paban. Bogoliubov Excited States and the Lyth Bound. *JCAP*, 1408:058, 2014.

[14] Aditya Aravind, Dustin Lorshbough, and Sonia Paban. Lower bound for the multifield bounce action. *Phys. Rev.*, D89(10):103535, 2014.

[15] Aditya Aravind, Dustin Lorshbough, and Sonia Paban. On primordial equation of state transitions. 2016.

[16] Aditya Aravind, Minglei Xiao, and Jiang-Hao Yu. Higgs Portal to Inflation and Fermionic Dark Matter. *Phys. Rev.*, D93(12):123513, 2016.

[17] Chiara Arina, Jinn-Ouk Gong, and Narendra Sahu. Unifying dark-lepto-genesis with scalar triplet inflation. *Nucl. Phys.*, B865:430–460, 2012.

[18] Seungwon Baek, P. Ko, Wan-Il Park, and Eibun Senaha. Vacuum structure and stability of a singlet fermion dark matter model with a singlet scalar messenger. *JHEP*, 11:116, 2012.

[19] Vijay Balasubramanian, Bartlomiej Czech, Klaus Larjo, and Thomas S. Levi. Vacuum decay in multidimensional field landscapes: thin, thick and intersecting walls. *Phys. Rev.*, D84:025019, 2011.

[20] J. L. F. Barbon and J. R. Espinosa. On the Naturalness of Higgs Inflation. *Phys. Rev.*, D79:081302, 2009.

[21] Daniel Baumann. Inflation. In *Physics of the large and the small, TASI 09, proceedings of the Theoretical Advanced Study Institute in Elementary Particle Physics, Boulder, Colorado, USA, 1-26 June 2009*, pages 523–686, 2011.

[22] F. Bezrukov, D. Gorbunov, and M. Shaposhnikov. On initial conditions for the Hot Big Bang. *JCAP*, 0906:029, 2009.

[23] F. Bezrukov, A. Magnin, M. Shaposhnikov, and S. Sibiryakov. Higgs inflation: consistency and generalisations. *JHEP*, 01:016, 2011.

[24] Fedor L. Bezrukov and Mikhail Shaposhnikov. The Standard Model Higgs boson as the inflaton. *Phys. Lett.*, B659:703–706, 2008.

[25] Raphael Bousso, Daniel Harlow, and Leonardo Senatore. Inflation After False Vacuum Decay: New Evidence from BICEP2. *JCAP*, 1412(12):019, 2014.

[26] Raphael Bousso, Daniel Harlow, and Leonardo Senatore. Inflation after False Vacuum Decay. *Phys. Rev.*, D91(8):083527, 2015.

[27] Raphael Bousso and Joseph Polchinski. Quantization of four form fluxes and dynamical neutralization of the cosmological constant. *JHEP*, 06:006, 2000.

[28] C. P. Burgess, Hyun Min Lee, and Michael Trott. Power-counting and the Validity of the Classical Approximation During Inflation. *JHEP*, 09:103, 2009.

[29] C. P. Burgess, Hyun Min Lee, and Michael Trott. Comment on Higgs Inflation and Naturalness. *JHEP*, 07:007, 2010.

[30] Dario Buttazzo, Giuseppe Degrassi, Pier Paolo Giardino, Gian F. Giudice, Filippo Sala, Alberto Salvio, and Alessandro Strumia. Investigating the near-criticality of the Higgs boson. *JHEP*, 12:089, 2013.

[31] Xavier Calmet and Roberto Casadio. Self-healing of unitarity in Higgs inflation. *Phys. Lett.*, B734:17–20, 2014.

[32] Daniel Carney, Willy Fischler, Sonia Paban, and Navin Sivanandam. The Inflationary Wavefunction and its Initial Conditions. *JCAP*, 1212:012, 2012.

[33] Girish Chakravarty, Subhendra Mohanty, and Naveen K. Singh. Higgs Inflation in $f(\Phi, R)$ Theory. *Int. J. Mod. Phys.*, D23(4):1450029, 2014.

[34] Serguei Chatrchyan et al. Search for a standard-model-like Higgs boson with a mass in the range 145 to 1000 GeV at the LHC. *Eur. Phys. J.*, C73:2469, 2013.

[35] Xingang Chen, Min-xin Huang, Shamit Kachru, and Gary Shiu. Observational signatures and non-Gaussianities of general single field inflation. *JCAP*, 0701:002, 2007.

[36] Diego Chialva. Signatures of very high energy physics in the squeezed limit of the bispectrum (violation of Maldacena's condition). *JCAP*, 1210:037, 2012.

[37] T. E. Clark, Boyang Liu, S. T. Love, and T. ter Veldhuis. The Standard Model Higgs Boson-Inflaton and Dark Matter. *Phys. Rev.*, D80:075019, 2009.

[38] Sidney R. Coleman. The Fate of the False Vacuum. 1. Semiclassical Theory. *Phys. Rev.*, D15:2929–2936, 1977. [Erratum: Phys. Rev.D16,1248(1977)].

[39] Sidney R. Coleman and Frank De Luccia. Gravitational Effects on and of Vacuum Decay. *Phys. Rev.*, D21:3305, 1980.

[40] Sidney R. Coleman, V. Glaser, and Andre Martin. Action Minima Among Solutions to a Class of Euclidean Scalar Field Equations. *Commun. Math. Phys.*, 58:211, 1978.

[41] Bartlomiej Czech. A Novel Channel for Vacuum Decay. *Phys. Lett.*, B713:331–334, 2012.

[42] Moumita Das and Subhendra Mohanty. Conformally invariant inert Higgs doublet model: An unified model for inflation and dark matter. *J. Phys. Conf. Ser.*, 405:012010, 2012.

[43] Giuseppe Degrassi, Stefano Di Vita, Joan Elias-Miro, Jose R. Espinosa, Gian F. Giudice, Gino Isidori, and Alessandro Strumia. Higgs mass and vacuum stability in the Standard Model at NNLO. *JHEP*, 08:098, 2012.

[44] Nathalie Deruelle and Viatcheslav F. Mukhanov. On matching conditions for cosmological perturbations. *Phys. Rev.*, D52:5549–5555, 1995.

[45] Melissa Duncan, Wei Gu, Yang-Hui He, and Da Zhou. The Statistics of Vacuum Geometry. *JHEP*, 06:042, 2014.

[46] Oscar J. P. Eboli, So-Young Pi, and M. Samiullah. Renormalizability of Functional Schrodinger Picture in Robertson-walker Space-time. *Annals Phys.*, 193:102, 1989.

[47] E. Elizalde and S. D. Odintsov. Renormalization group improved effective Lagrangian for interacting theories in curved space-time. *Phys. Lett.*, B321:199–204, 1994.

[48] E. Elizalde, S. D. Odintsov, E. O. Pozdeeva, and S. Yu. Vernov. Renormalization-group improved inflationary scalar electrodynamics and SU(5) scenarios confronted with Planck 2013 and BICEP2 results. *Phys. Rev.*, D90(8):084001, 2014.

[49] John R. Ellis, Andrew Ferstl, and Keith A. Olive. Reevaluation of the elastic scattering of supersymmetric dark matter. *Phys. Lett.*, B481:304–314, 2000.

[50] Malcolm Fairbairn and Robert Hogan. Singlet Fermionic Dark Matter and the Electroweak Phase Transition. *JHEP*, 09:022, 2013.

[51] Jonathan L. Feng, John March-Russell, Savdeep Sethi, and Frank Wilczek. Saltatory relaxation of the cosmological constant. *Nucl. Phys.*, B602:307–328, 2001.

[52] A. Ferraz de Camargo, R. C. Shellard, and G. C. Marques. Vacuum Decay in a Soluble Model. *Phys. Rev.*, D29:1147, 1984.

[53] Raphael Flauger, Daniel Green, and Rafael A. Porto. On squeezed limits in single-field inflation. Part I. *JCAP*, 1308:032, 2013.

[54] Ben Freivogel. Making predictions in the multiverse. *Class. Quant. Grav.*, 28:204007, 2011.

[55] Ben Freivogel, Matthew Kleban, Maria Rodriguez Martinez, and Leonard Susskind. Observational consequences of a landscape. *JHEP*, 03:039, 2006.

[56] Sergio Fubini. A New Approach to Conformal Invariant Field Theories. *Nuovo Cim.*, A34:521, 1976.

[57] Jonathan Ganc. Calculating the local-type fNL for slow-roll inflation with a non-vacuum initial state. *Phys. Rev.*, D84:063514, 2011.

[58] Jonathan Ganc and Eiichiro Komatsu. A new method for calculating the primordial bispectrum in the squeezed limit. *JCAP*, 1012:009, 2010.

[59] Cristiano Germani and Alex Kehagias. Cosmological Perturbations in the New Higgs Inflation. *JCAP*, 1005:019, 2010. [Erratum: JCAP1006,E01(2010)].

[60] Gian F. Giudice and Hyun Min Lee. Unitarizing Higgs Inflation. *Phys. Lett.*, B694:294–300, 2011.

[61] Paolo Gondolo and Graciela Gelmini. Cosmic abundances of stable particles: Improved analysis. *Nucl. Phys.*, B360:145–179, 1991.

[62] Jinn-Ouk Gong, Hyun Min Lee, and Sin Kyu Kang. Inflation and dark matter in two Higgs doublet models. *JHEP*, 04:128, 2012.

[63] Jinn-Ouk Gong and Misao Sasaki. Squeezed primordial bispectrum from general vacuum state. *Class. Quant. Grav.*, 30:095005, 2013.

[64] Brian Greene, David Kagan, Ali Masoumi, Dhagash Mehta, Erick J. Weinberg, and Xiao Xiao. Tumbling through a landscape: Evidence of instabilities in high-dimensional moduli spaces. *Phys. Rev.*, D88(2):026005, 2013.

[65] Brian R. Greene, Koenraad Schalm, Gary Shiu, and Jan Pieter van der Schaar. Decoupling in an expanding universe: Backreaction barely constrains short distance effects in the CMB. *JCAP*, 0502:001, 2005.

[66] Kim Griest and David Seckel. Three exceptions in the calculation of relic abundances. *Phys. Rev.*, D43:3191–3203, 1991.

[67] Alan H. Guth. Eternal inflation and its implications. *J. Phys.*, A40:6811–6826, 2007.

[68] Naoyuki Haba, Hiroyuki Ishida, and Ryo Takahashi. Higgs inflation and Higgs portal dark matter with right-handed neutrinos. *PTEP*, 2015(5):053B01, 2015.

[69] Yuta Hamada, Hikaru Kawai, and Kin-ya Oda. Predictions on mass of Higgs portal scalar dark matter from Higgs inflation and flat potential. *JHEP*, 07:026, 2014.

[70] Yuta Hamada, Kin-ya Oda, and Fuminobu Takahashi. Topological Higgs inflation: Origin of Standard Model criticality. *Phys. Rev.*, D90(9):097301, 2014.

[71] S. H. Henry Tye, Daniel Wohns, and Yang Zhang. Coleman-de Luccia Tunneling and the Gibbons-Hawking Temperature. *Int. J. Mod. Phys.*, A25:1019–1060, 2010.

[72] Mark P. Hertzberg. On Inflation with Non-minimal Coupling. *JHEP*, 11:023, 2010.

[73] R. Holman and Andrew J. Tolley. Enhanced Non-Gaussianity from Excited Initial States. *JCAP*, 0805:001, 2008.

[74] Fa Peng Huang, Chong Sheng Li, Ding Yu Shao, and Jian Wang. Phenomenology of an Extended Higgs Portal Inflation Model after Planck 2013. *Eur. Phys. J.*, C74(8):2990, 2014.

[75] Matthew C. Johnson and Magdalena Larfors. Field dynamics and tunneling in a flux landscape. *Phys. Rev.*, D78:083534, 2008.

[76] Marc Kamionkowski and Ely D. Kovetz. The Quest for B Modes from Inflationary Gravitational Waves. 2015.

[77] Kristjan Kannike, Gert Htsi, Liberato Pizza, Antonio Racioppi, Martti Raidal, Alberto Salvio, and Alessandro Strumia. Dynamically Induced Planck Scale and Inflation. *JHEP*, 05:065, 2015.

[78] Valentin V. Khoze. Inflation and Dark Matter in the Higgs Portal of Classically Scale Invariant Standard Model. *JHEP*, 11:215, 2013.

[79] Yeong Gyun Kim, Kang Young Lee, and Seodong Shin. Singlet fermionic dark matter. *JHEP*, 05:100, 2008.

[80] Thomas Konstandin and Stephan J. Huber. Numerical approach to multi dimensional phase transitions. *JCAP*, 0606:021, 2006.

[81] Sandipan Kundu. Inflation with General Initial Conditions for Scalar Perturbations. *JCAP*, 1202:005, 2012.

[82] Sandipan Kundu. Non-Gaussianity Consistency Relations, Initial States and Back-reaction. *JCAP*, 1404:016, 2014.

[83] Oleg Lebedev and Hyun Min Lee. Higgs Portal Inflation. *Eur. Phys. J.*, C71:1821, 2011.

[84] Rose N. Lerner and John McDonald. Higgs Inflation and Naturalness. *JCAP*, 1004:015, 2010.

[85] Rose N. Lerner and John McDonald. Unitarity-Violation in Generalized Higgs Inflation Models. *JCAP*, 1211:019, 2012.

[86] Rose Natalie Lerner and John McDonald. Gauge singlet scalar as inflaton and thermal relic dark matter. *Phys. Rev.*, D80:123507, 2009.

[87] Tai Li and Yu-Feng Zhou. Strongly first order phase transition in the singlet fermionic dark matter model after LUX. *JHEP*, 07:006, 2014.

[88] Andrei D. Linde. Decay of the False Vacuum at Finite Temperature. *Nucl. Phys.*, B216:421, 1983. [Erratum: Nucl. Phys.B223,544(1983)].

[89] Andrei D. Linde. Quantum creation of an open inflationary universe. *Phys. Rev.*, D58:083514, 1998.

[90] Farhang Loran. Fubini vacua as a classical de Sitter vacua. *Mod. Phys. Lett.*, A22:2217–2235, 2007.

[91] Juan Martin Maldacena. Non-Gaussian features of primordial fluctuations in single field inflationary models. *JHEP*, 05:013, 2003.

[92] Ali Masoumi and Erick J. Weinberg. Bounces with O(3) x O(2) symmetry. *Phys. Rev.*, D86:104029, 2012.

[93] Sander Mooij and Marieke Postma. Goldstone bosons and a dynamical Higgs field. *JCAP*, 1109:006, 2011.

[94] Kazunori Nakayama and Fuminobu Takahashi. Higgs Chaotic Inflation in Standard Model and NMSSM. *JCAP*, 1102:010, 2011.

[95] Nobuchika Okada and Qaisar Shafi. Higgs Inflation, Seesaw Physics and Fermion Dark Matter. *Phys. Lett.*, B747:223–228, 2015.

[96] Daniel S. Park. Scalar Three-point Functions in a CDL Background. *JHEP*, 01:165, 2012.

[97] Tomislav Prokopec and Jan Weenink. Naturalness in Higgs inflation in a frame independent formalism. 2014.

[98] Hong-Yi Qin, Wen-Yu Wang, and Zhao-Hua Xiong. A simple singlet fermionic dark-matter model revisited. *Chin. Phys. Lett.*, 28:111202, 2011.

[99] Alberto Salvio. Higgs Inflation at NNLO after the Boson Discovery. *Phys. Lett.*, B727:234–239, 2013.

[100] Sash Sarangi, Gary Shiu, and Benjamin Shlaer. Rapid Tunneling and Percolation in the Landscape. *Int. J. Mod. Phys.*, A24:741–788, 2009.

[101] Uri Sarid. Tools for tunneling. *Phys. Rev.*, D58:085017, 1998.

[102] Claudio Scrucca. Advanced quantum field theory - doctoral school in physics, epfl.

[103] Eva Silverstein and Alexander Westphal. Monodromy in the CMB: Gravity Waves and String Inflation. *Phys. Rev.*, D78:106003, 2008.

[104] Kazuyuki Sugimura and Eiichiro Komatsu. Bispectrum from open inflation. *JCAP*, 1311:065, 2013.

[105] S. H. Henry Tye and Daniel Wohns. Resonant Tunneling in Scalar Quantum Field Theory. 2009.

[106] Carroll L. Wainwright. CosmoTransitions: Computing Cosmological Phase Transition Temperatures and Bubble Profiles with Multiple Fields. *Comput. Phys. Commun.*, 183:2006–2013, 2012.

[107] Erick J. Weinberg. *Classical solutions in quantum field theory.* Cambridge Monographs on Mathematical Physics. Cambridge University Press, 2015.

[108] Ming-Lei Xiao and Jiang-Hao Yu. Stabilizing electroweak vacuum in a vectorlike fermion model. *Phys. Rev.*, D90(1):014007, 2014. [Addendum: Phys. Rev.D90,no.1,019901(2014)].

[109] Daisuke Yamauchi, Andrei Linde, Atsushi Naruko, Misao Sasaki, and Takahiro Tanaka. Open inflation in the landscape. *Phys. Rev.*, D84:043513, 2011.

[110] Hongsheng Zhang, Yi Zhang, and Xin-Zhou Li. Higgs inflation on braneworld. *Mod. Phys. Lett.*, A29(08):1450039, 2014.